Clinopyroxene archives of magma redox in ocean island basalts: insights from thermodynamic modelling

David A. Neave[1]*, Owen M. Weller[2] and Caroline R. Soderman[2]

[1]Department of Earth and Environmental Sciences, University of Manchester, Oxford Road, Manchester, M13 9PL, United Kingdom

[2]Department of Earth Sciences, University of Cambridge, Downing Street, Cambridge, CB2 3EQ, United Kingdom

*Corresponding author: david.neave@manchester.ac.uk

Short title: Thermodynamic insights into clinopyroxene records of magma redox

Key words: redox, ocean island basalt, thermodynamic modelling, clinopyroxene

Abstract

Iron plays a central role in both setting and recording magma redox states, which are commonly expressed as oxygen fugacity (f_{O_2}) deviations away from known equilibria such as fayalite-magnetite-quartz (FMQ). Magmas erupted in different settings are often characterised by different f_{O_2} conditions, with the f_{O_2} conditions experienced by ocean island basalts (OIBs) being especially variable and difficult to determine. Current tools for estimating magmatic f_{O_2} conditions are subject to diverse limitations and can rarely be applied across a wide range of sample types. This makes it challenging to draw conclusions about the nature and origins of f_{O_2} variability within and between magmatic systems. Recent work has demonstrated how analysing clinopyroxene crystals containing Fe^{2+} and Fe^{3+} could potentially offer a new way to investigate variability in both Fe valence (i.e., $Fe^{3+}/\Sigma Fe$, where $\Sigma Fe = Fe^{2+} + Fe^{3+}$) and f_{O_2} conditions within and between magmas. However, relating clinopyroxene $Fe^{3+}/\Sigma Fe$ contents to magmatic f_{O_2} conditions is challenging because of the steric effects imposed by the structure of clinopyroxene crystals. Given the current paucity of experimental observations capable of separating steric controls over clinopyroxene $Fe^{3+}/\Sigma Fe$ contents from those imposed by magmatic f_{O_2} conditions, we report the results of pseudosection modelling performed with recently developed thermodynamic models that allow us to parameterise sample-wise relationships between clinopyroxene $Fe^{3+}/\Sigma Fe$ contents and magmatic f_{O_2} conditions. By combining pseudosection modelling results with observations from natural samples, we estimate pre-eruptive f_{O_2} conditions of FMQ to FMQ+0.6 for two tholeiitic basalts from Iceland and FMQ+1.1 for a trachybasaltic-to-tephritic sample from Pico Island in the Azores. The former two values are consistent with previous estimates from Icelandic samples suggesting magmatic evolution under conditions slightly more oxidising than mid-ocean ridge basalts. The latter value is slightly more reducing than many estimates from systems that are geochemically similar to the Azores, suggesting that the values we calculate may have been compromised by reductive SO_2 degassing. Although further experimental work is required to refine thermodynamic models of clinopyroxene behaviour, especially in alkalic systems, our results nonetheless highlight how integrating thermodynamic models and natural observations can provide new insights into magma redox.

Introduction

Iron is the most abundant multivalent element in terrestrial magmas and thus plays a central role in both setting and recording magma redox (Frost, 1991); all else being equal, the higher the ferric-to-total Fe (i.e., $Fe^{3+}/\Sigma Fe$) content of a magma, the more oxidising

it will be. In turn, magma redox, which is generally expressed in terms of oxygen fugacity (f_{O_2}), affects phase equilibria, volatile solubilities, magma evolution trajectories and the composition of volcanic gas emissions (e.g., Toplis & Carroll, 1995; Burgisser & Scaillet, 2007; Jugo, 2009; Feig *et al.*, 2010; Hughes *et al.*, 2023). Understanding how magmatic f_{O_2} varies in space and time is therefore central to understanding processes that range from the formation of ore deposits to the maintenance of planetary habitability (e.g., Holland, 2002; Evans & Tomkins, 2011). Observations made over several decades suggest that arc basalts typically evolve under more oxidising conditions than mid-ocean ridge basalts (MORBs; Wood *et al.*, 1990; Carmichael, 1991; Cottrell *et al.*, 2022). That is, MORBs are thought to evolve under f_{O_2} conditions close to fayalite-magnetite-quartz (∼FMQ) equilibrium, while arc basalts are thought to evolve under f_{O_2} conditions approximately one log unit above FMQ equilibrium (FMQ+1), even though the ultimate cause(s) of this ridge-arc dichotomy remain contested (Gaetani, 2016; Brounce *et al.*, 2019; Evans & Tomkins, 2022). In contrast, ocean island basalts (OIBs) present a more complex picture, with observations from the Canary Islands and Mount Erebus indicating OIB evolution under f_{O_2} conditions two log units or more above FMQ equilibrium (≥FMQ+2; Moussallam *et al.*, 2014, 2019; Taracsák *et al.*, 2022; Nicklas *et al.*, 2022b), observations from Réunion indicating OIB evolution under f_{O_2} conditions at or even below FMQ equilibrium (≤FMQ; Brounce *et al.*, 2022; Nicklas *et al.*, 2022a) and observations from other settings including Iceland and Hawaii indicating OIB evolution under conditions between these extremes (Brounce *et al.*, 2017; Helz *et al.*, 2017; Hartley *et al.*, 2017). Compositional differences between different mantle end-members have been invoked as a potential explanation for the apparent variability in OIB f_{O_2} conditions, with EM-I, EM-II and HIMU sources thought to be especially oxidised (Brounce *et al.*, 2022). However, generating the internally consistent datasets needed to study magma redox variability systematically is challenging because different oxybarometers with different uncertainties and limitations (e.g., glass $Fe^{3+}/\Sigma Fe$ contents, magnetite-ilmenite pairs, spinel compositions and olivine V contents) have been applied in separate settings over recent decades (e.g., Cottrell *et al.*, 2022). This status quo arises because different OIBs contain distinct phase assemblages and are subject to unique magmatic and secondary processes that make it difficult to apply any individual oxybarometer across a wide range of samples. For example, both pristine mantle-derived glasses and equilibrium magnetite-ilmenite pairs are rare in many OIB settings. A different approach for estimating magma redox conditions based on widely occurring and chemically robust phases would thus be highly valuable tool for interrogating redox variability in OIB settings.

Clinopyroxene is a major constituent of magmas erupted across all tectonic settings.

Depending on the prevailing conditions, clinopyroxene, which has the formula M2(R^{2+}) M1(R^{2+})T_2($2R^{4+}$)O_6 (where R is a metal cation, M2 is a distorted octahedral site, M1 is a regular octahedral site and T is a tetrahedral site), can contain significant quantities of both Fe^{2+} and Fe^{3+} (Morimoto *et al.*, 1988). For example, Fe^{3+} is typically incorporated into augitic clinopyroxene crystals (Ca(Mg,Fe^{2+})Si_2O_6) via Tschermak-type substitutions—M1(R^{2+})T(R^{4+})–M1(R^{3+})T(R^{3+})—such as (Mg,Fe^{2+})Si–Fe^{3+}Al (Luth & Canil, 1993; Neave *et al.*, 2019a; Chicchi *et al.*, 2023). It follows that clinopyroxene $Fe^{3+}/\Sigma Fe$ contents should reflect magma $Fe^{3+}/\Sigma Fe$ contents (steric constraints and diffusive overprinting notwithstanding), and may hence offer a new way to investigate f_{O_2} variations within and between magmatic systems. However, determining clinopyroxene $Fe^{3+}/\Sigma Fe$ contents accurately and precisely has traditionally proven challenging, with unfavourable assessments of stoichiometric approaches meaning that Mössbauer spectroscopy has generally been deemed necessary to estimate clinopyroxene $Fe^{3+}/\Sigma Fe$ contents with sufficient rigour to address geological problems (McGuire *et al.*, 1989; Canil & O'Neill, 1996; Sobolev *et al.*, 1999). Fortunately, Neave *et al.* (2024a) recently demonstrated that the $Fe^{3+}/\Sigma Fe$ content of magmatic clinopyroxene crystals containing moderate amounts of Fe (i.e., more than a few wt.% FeO^T, where FeO^T is total Fe expressed as FeO) can be estimated from stoichiometric constraints as long as electron probe microanalysis (EPMA) is carried out with sufficient care. Thus, Neave *et al.* (2024b) subsequently demonstrated that clinopyroxene crystals from OIBs erupted in Iceland and the Azores contain appreciable quantities of Fe^{3+} (up to ~4 wt.% when expressed as Fe_2O_3) that correspond to $Fe^{3+}/\Sigma Fe$ contents up to ~0.4. By evaluating Fe^{2+}–Mg exchange equilibria using experimentally derived $K_{D,Fe^{2+}-Mg}^{cpx-liq}$ values of ~0.24 (Pilet *et al.*, 2010; Salazar-Naranjo & Vlach, 2023), they observed that mean clinopyroxene compositions unaffected by reductive SO_2 degassing recorded f_{O_2} conditions of ~FMQ+1 in tholeiitic basalts from Iceland and ~FMQ+2.5 in alkali basalts from the Azores, in line with published observations from compositionally similar systems (e.g., Hartley *et al.*, 2017; Moussallam *et al.*, 2019). However, steric constraints imposed by clinopyroxene crystal structures mean that relationships between clinopyroxene $Fe^{3+}/\Sigma Fe$ content and f_{O_2} conditions are more complex than relationships between glass $Fe^{3+}/\Sigma Fe$ contents and f_{O_2} conditions. Given the current paucity of experimental products equilibrated at a range of f_{O_2} conditions and measured with sufficient precision to robustly estimate clinopyroxene $Fe^{3+}/\Sigma Fe$ contents by stoichiometry, a different approach is needed to relate magmatic f_{O_2} conditions to clinopyroxene $Fe^{3+}/\Sigma Fe$ contents.

Thermodynamic models provide key tools for extrapolating phase equilibria relations into pressure-temperature-bulk composition (P–T–X) conditions that are yet to be ex-

perimentally studied in detail and thus offer considerable untapped potential for interpreting crystal records of magmatic f_{O_2} conditions. The calculation of pseudosections that describe equilibrium phase relations for a given bulk composition is a well established approach for understanding the petrogenesis of metamorphic rocks (Powell & Holland, 2008). Recent work on expanding calibration ranges of composition-dependent equations of state (x-eos) for the melt phase, alongside continued development of solid phase x-eos, now means that pseudosections can be calculated for igneous systems that range in composition from ultramafic to felsic (e.g., Jennings & Holland, 2015; Green *et al.*, 2016; Holland *et al.*, 2018; Tomlinson & Holland, 2021). A recent expansion of x-eos into alkaline-silicate systems via extending the calibration ranges of existing models and calibrating new models for key phases in alkali-rich systems (e.g., nepheline) also means that a wide spectrum of silica-undersaturated (i.e., nepheline-normative) OIBs can be modelled (Weller *et al.*, 2024). Moreover, the development of a new Gibbs free energy minimisation algorithm, known as MAGEMin, has drastically reduced the time required to calculate pseudosections by employing single-point calculation parallelisation (Riel *et al.*, 2022). It is thus now feasible to use pseudosection modelling to explicitly account for steric controls over clinopyroxene compositions, enabling clinopyroxene $Fe^{3+}/\Sigma Fe$ contents to be directly related to magmatic f_{O_2} conditions by calculating pseudosections at a range of bulk $Fe^{3+}/\Sigma Fe$ contents (referred to here as $X_{Fe^{3+}}$ values) on a sample-by-sample basis. Furthermore, taking an equilibrium thermodynamics approach also allows for kinetic controls over clinopyroxene compositions to be identified and excluded when interpreting natural datasets (cf., Mollo *et al.*, 2013; Neave *et al.*, 2019a; Ubide *et al.*, 2019; MacDonald *et al.*, 2023).

Here we present the results of pseudosection modelling performed on four OIB bulk compositions, two from Iceland and two from the Azores, for which high-precision analyses of clinopyroxene crystals were recently published (Neave *et al.*, 2024b). Our results allow us to estimate equilibrium $D^{cpx-liq}_{Fe^{3+}}$ and $K^{cpx-liq}_{D,Fe^{2+}-Mg}$ values, though also highlight the challenges associated with describing Fe^{3+} exchange behaviour with simple partition coefficients as well as our still poor understanding of Fe^{2+}–Mg exchange between clinopyroxene and magmatic liquids. They nevertheless enable us to demonstrate that differences in clinopyroxene $Fe^{3+}/\Sigma Fe$ contents partly reflect differences in bulk composition as well as differences in prevailing f_{O_2} conditions, with our compositions from the Azores recording magmatic evolution under more oxidising conditions than those from Iceland.

Modelling approach

In order to disentangle the effects of T, X and f_{O_2} on clinopyroxene $Fe^{3+}/\Sigma Fe$ contents, we performed T–$X_{Fe^{3+}}$ pseudosection modelling on four OIB bulk compositions thought to have evolved under different f_{O_2} conditions but relatively well known P conditions (Neave *et al.*, 2024b). By calculating isobaric pseudosections at a range of T–$X_{Fe^{3+}}$ conditions, we can explore the sensitivity of clinopyroxene $Fe^{3+}/\Sigma Fe$ contents to f_{O_2} and implicitly account for steric controls over clinopyroxene compositions. Of the OIB samples investigated by Neave *et al.* (2024b), we focus here on two tholeiitic samples from Iceland (one tephra sample from the Holuhraun eruption and one lava sample from the Laki eruption) and two alkalic samples from Pico Island in the Azores (one alkali basalt lava sample (PI-011) and one trachybasaltic-to-tephritic tephra sample (PI-041); Fig 1). These samples likely formed under a range of f_{O_2} conditions (potentially ~FMQ+1 to ~FMQ+2.5; Neave *et al.*, 2024b) characteristic of global OIBs (e.g., Brounce *et al.*, 2017; Hartley *et al.*, 2017; Moussallam *et al.*, 2019; Taracsák *et al.*, 2022). They also span a range of alkali contents and degrees of evolution, with our sample from the Holuhraun eruption and sample PI-011 from Pico being relatively primitive (high Mg# values, where Mg# = $Mg/(Mg+Fe^{2+})$ on a molar basis), and our sample from the Laki eruption and sample PI-041 from Pico being relatively evolved (low Mg# values). In the case of the Holuhraun eruption we augmented the high-precision EPMA dataset reported by Neave *et al.* (2024b) with a lower precision but nevertheless modern and voluminous dataset reported by Halldórsson *et al.* (2018).

Model bulk compositions used as inputs for the pseudosection calculations were based on the compositions provided in Table 1. Bulk compositions for the Holuhraun and Laki eruptions reflect mean whole-rock compositions reported by Halldórsson *et al.* (2018) and Passmore *et al.* (2012), respectively; bulk compositions for samples PI-011 and PI-041 from Pico were taken from the whole-rock compositions reported by van Gerve *et al.* (2024). We calculated pseudosections from whole-rock compositions rather than matrix glass compositions because our ultimate aim is to estimate magmatic f_{O_2} conditions from clinopyroxene crystals grown from carrier liquids now represented by matrix glasses. As such, if we calculated pseudosections from matrix glass compositions, then modelled clinopyroxene compositions could never correspond directly to measured clinopyroxene compositions. Nevertheless, this approach assumes that modelled whole-rock compositions are simple mixtures of quenched matrix glasses and their equilibrium crystal assemblages. We therefore initially assume that our whole-rock compositions reflect true magmatic liquids and are unaffected by crystal accumulation processes (cf., Neave *et al.*, 2014; Ubide *et al.*, 2014). This assumption has been broadly verified for the Holuhraun eruption whose

products contain little accumulated or antecrystic material (Halldórsson *et al.*, 2018). In contrast, the products of the Laki eruption appear to contain some crystals entrained from mushes (Passmore *et al.*, 2012; Neave *et al.*, 2013). However, the mean crystal content of the Laki lava is modest (∼12 vol.%), meaning that any effects of crystal accumulation on our pseudosection calculations will be comparably minor. The impacts of potential crystal accumulation on PI-011 and PI-041 are less well understood, though van Gerve *et al.* (2024) noted that many of their samples from Pico contain abundant olivine and clinopyroxene macrocrysts, and that whole-rock compositions containing >10 wt.% MgO may have accumulated mafic minerals (e.g., Ubide *et al.*, 2022). As such, the whole-rock composition for PI-011 may have experienced accumulation. In a subsequent section we describe the approach used to verify equilibrium between our modelled compositions and natural compositions from Neave *et al.* (2024b) and avoid misinterpretations arising from basing assumptions on unrealistic magma compositions.

Pseudosections were calculated using THERMOCALC v3.51s (Powell *et al.*, 1998) with version 6.36 of the Holland & Powell (2011) thermodynamic dataset, as described by Weller *et al.* (2024). Pseudosection topologies were verified by initial calculations performed with MAGEMin (Riel *et al.*, 2022). Calculations were performed in the anhydrous nine-component Na_2O–CaO–K_2O–FeO–MgO–Al_2O_3–SiO_2–TiO_2–Fe_2O_3 (NCKFMASTO) model system using x-eos models from Weller *et al.* (2024) for all phases except feldspar (Holland *et al.*, 2022), olivine (Holland *et al.*, 2018) and spinel (Tomlinson & Holland, 2021). To explore the general effects of H_2O on phase relations and compositions in light of the results obtained with the anhydrous modelling desvribed above, we also performed targeted modelling on the sub-alkaline Holuhraun bulk compositions in a hydrous system (Na_2O–CaO–K_2O–FeO–MgO–Al_2O_3–SiO_2–H_2O–TiO_2–Fe_2O_3; NCKFMASHTO) using the hydrous granitic to ultramafic melt x-eos model described in (Holland *et al.*, 2018) in place of the extended alkali melt model of Weller *et al.* (2024). The latter melt model was calibrated using the same constraints as Holland *et al.* (2018) so outputs between the two models are comparable; both models are required as no single model can currently be used for both alkaline and hydrous compositions. Model inputs (expressed on a molar basis) are provided in Table 2. Components outside the model system (i.e., MnO and P_2O_5) are ignored when converting to the model system. We chose not to perform an apatite correction to CaO concentrations based on P_2O_5 contents (Weller *et al.*, 2013) because we are investigating systems at temperatures at which apatite not stable (Watson, 1979). As discussed by Weller *et al.* (2024), f_{O_2} is internally buffered in natural systems by the phase assemblage present, which contrasts with the external buffering than can be imposed on experimental systems. To provide a common frame of reference, internally buffered f_{O_2}

conditions can be expressed relative to any given equilibria; here we report f_{O_2} conditions as log-unit deviations from FMQ equilibrium. This calculation was achieved by determining equilibria between model end-members that involve O_2, such as 4hmL + 2/3q3L = fa2L + O_2. G_{O_2} and $\log(f_{O_2})$ with respect to FMQ were then calculated from the Holland & Powell (2011) dataset. All mineral name abbreviations follow the guidelines provided in Weller *et al.* (2024).

All pseudosections were calculated from superliquidus to solidus temperatures (typically 950–1250 °C) and with initial $X_{Fe^{3+}}$ values ranging from 0.0 to 0.4 that encompass the range of liquid $Fe^{3+}/\Sigma Fe$ conditions reported from global OIB systems (Moussallam *et al.*, 2019; Brounce *et al.*, 2022; Cottrell *et al.*, 2022). Calculations on our tholeiitic bulk compositions from Holuhraun and Laki were performed at 300 MPa based on thermobarometric estimates of pre-eruptive magma storage conditions that lie in the 200–400 MPa range (Neave *et al.*, 2013; Neave & Putirka, 2017; Halldórsson *et al.*, 2018). Conversely, calculations on our alkalic bulk compositions from Pico were performed at 500 MPa based on estimated magma storage conditions beneath the island as a whole (van Gerve *et al.*, 2024). Although magmas are often stored and processed at a range of pressures prior to eruption, we focus primarily on evaluating the composition of clinopyroxene crystals in equilibrium with erupted liquids, and as such do not consider the phase relations of parental magmas feasibly stored at greater pressures. Moreover, the effects of modest discrepancies between real and modelled storage pressures (perhaps on the order of 100 MPa) are unlikely to resolvable given the similar size of uncertainties in pseudosection calculations (Palin *et al.*, 2016; Weller *et al.*, 2024).

Modelling results

Pseudosections

Isobaric T–$X_{Fe^{3+}}$ pseudosections calculated for our four bulk compositions are shown in Fig. 2, with equivalent diagrams contoured for f_{O_2} shown in Fig. 3. Pseudosections calculated for bulk compositions from the Holuhraun and Laki eruptions (Figs. 2A and 2B, respectively) show similar topologies, consistent with these eruptions both being tholeiitic basalts from Iceland's axial rift. Clinopyroxene is the liquidus phase for both compositions across the full range of modelled $X_{Fe^{3+}}$ values, followed by plagioclase. This result is consistent with the prevalence of these phases in natural samples and the fact that both compositions are at least somewhat evolved (6.8 and 5.8 wt.% MgO respectively), such that the amount of olivine expected to crystallise from these compositions is low or negli-

gible (Neave *et al.*, 2019b); much of the olivine in natural samples may represent crystals inherited from parental magmas that have experienced varying degrees of diffusive re-equilibration. Olivine does occur below the liquidus in both pseudosections at low $X_{Fe^{3+}}$ (<0.11 and <0.02 for Holuhraun and Laki, respectively), but is generally replaced by orthopyroxene (±pigeonite) at higher $X_{Fe^{3+}}$. Indeed, orthopyroxene (and pigeonite) may incorporated as disequilibrium Ca-poor components within augitic clinopyroxene crystals in natural samples since discrete orthopyroxene (or pigeonite) crystals are not observed in the products of either the Holuhraun or Laki eruptions; augitic clinopyroxene is also modally dominant over orthopyroxene and pigeonite in the results of pseudosection calculations (Figs. 4–7). The main difference between the Holuhraun and Laki pseudosections is that the former is characterised by a higher liquidus temperature (1190 versus 1160 °C), consistent with Holuhraun being more primitive. At lower temperatures, ilmenite and magnetite both occur, with their respective stabilities controlled by $X_{Fe^{3+}}$ (ilmenite more stable at low $X_{Fe^{3+}}$ and magnetite more stable at high $X_{Fe^{3+}}$; Shepherd *et al.*, 2022). Finally, quartz is stable just above the solidus at somewhat elevated $X_{Fe^{3+}}$ in both compositions, consistent with their compositions being silica saturated.

Pseudosections calculated for samples PI-011 and PI-041 from Pico in the Azores (Figs. 2C and 2D, respectively) show differences in topology both with respect to each other and with respect to the pseudosections calculated for Icelandic tholeiites. Olivine is the liquidus phase for PI-011 at a relatively elevated temperature of ∼1245–1285 °C depending on $X_{Fe^{3+}}$. The high temperature at which olivine is stabilised suggests that the bulk composition of PI-011 has been affected by the accumulation of mafic phases. As expected for an alkali basalt evolving at moderately high pressures (500 MPa), clinopyroxene is the next stable phase, followed by plagioclase; orthopyroxene is only stable at relatively high $X_{Fe^{3+}}$ values (>0.35). Consistent with sample petrography, magnetite and ilmenite occur at lower temperatures. Leucite is a near-solidus phase at all values of $X_{Fe^{3+}}$ modelled, and nepheline is present at low $X_{Fe^{3+}}$ (<0.05), in line with the bulk composition being silica undersaturated. In contrast, plagioclase is the liquidus phase for PI-041, with olivine (at $X_{Fe^{3+}} < 0.25$) or orthopyroxene (at $X_{Fe^{3+}} > 0.25$) and then clinopyroxene joining within a ∼50 °C interval. The occurrence of plagioclase as the liquidus phase is unexpected for an alkalic bulk composition (PI-041 is trachybasaltic-to-tephritic in composition); we speculate that our current inability to model hydrous alkalic systems may account for this result (though plagioclase accumulation could also play a role). Specifically, the H_2O content of mafic alkaline magmas from Pico reaches up to ∼1.5 wt.% (van Gerve *et al.*, 2024), a H_2O content capable of depressing the plagioclase liquidus by as much as 80 °C in tholeiitic systems (Almeev *et al.*, 2012). Indeed, illustrative pseudosection modelling performed

on the tholeiitic Holuhraun bulk composition with the H_2O-sensitive x-eos melt model from Holland *et al.* (2018) at a fixed $X_{Fe^{3+}}$ of 0.15 and H_2O contents of 0–2 wt.% H_2O demonstrate that increasing magma H_2O contents reduces plagioclase stability more than it reduces clinopyroxene stability (Supplementary Fig. 1). Two pigeonite solvii appear below the clinopyroxene liquidus, though, as for our tholeiitic compositions, we suggest in nature kinetic effects mean that these compositions are likely to be incorporated as low-Ca components within natural crystals; the modal abundance of pigeonite in these regions is also trivial when compared with that of augitic clinopyroxene. Ilmenite and magnetite show broadly similar behaviours to those modelled for PI-011. Potassium feldspar occurs near the liquidus at all $X_{Fe^{3+}}$ values modelled, and leucite occurs at low $X_{Fe^{3+}}$ values (<0.09).

Phase proportions, phase compositions, exchange reactions and oxygen fugacity conditions

Phase proportions, phase compositions, partitioning behaviours and f_{O_2} conditions of T–$X_{Fe^{3+}}$ slices through our calculated pseudosections are shown in Figs. 4–7 for modal proportions of liquid that range from 1 to 0.4. These T–$X_{Fe^{3+}}$ slices focus on near-liquidus phase relations because the ultimate aim of our study is to use pseudosection calculations to estimate magmatic f_{O_2} conditions from natural clinopyroxene compositions, with equilibrium clinopyroxene compositions most likely to have formed from liquids only slightly more evolved than the modelled bulk systems. In other words, we assume that equilibrium in our natural samples is most likely to be reflected by the near-liquidus phase relations in our model systems. Furthermore, by focusing on near-liquidus compositions we avoid introducing additional complications associated with using equilibrium calculations to interpret natural systems evolving by fractional crystallisation as differences between equilibrium and fractional systems are modest or negligible at high liquid proportions (Neave *et al.*, 2019b). Given that our alkalic samples are expected to have evolved under slightly higher f_{O_2} conditions than our tholeiitic bulk compositions (Hartley *et al.*, 2017; Bali *et al.*, 2018; Moussallam *et al.*, 2019; Brounce *et al.*, 2022; Neave *et al.*, 2024b), we present T–$X_{Fe^{3+}}$ slices at $X_{Fe^{3+}}$ = 0.15, 0.25 and 0.35 for the former and 0.10, 0.15 and 0.20 for the latter. These slices correspond to f_{O_2} conditions of ∼FMQ+0.1, ∼FMQ+1.3 and ∼FMQ+2.0, and ∼FMQ−0.5, ∼FMQ+0.3 and ∼FMQ+0.8, respectively (Fig. 3).

Equilibrium phase proportions evolve similarly as functions of decreasing temperature at fixed $X_{Fe^{3+}}$ values in both tholeiitic bulk compositions (e.g., Figs. 4A and 5A), with crystal stabilities in the relatively evolved Laki composition offset to lower temperatures

than those in the relatively primitive Holuhraun composition. Clinopyroxene and plagioclase modally dominate the solid assemblage at modal proportions of liquid >0.4, with clinopyroxene being slightly more abundant than plagioclase; modally minor combinations of orthopyroxene, magnetite and/or ilmenite are stable at lower temperatures when modal proportions of liquid proportions decrease below ~0.6. Clinopyroxene and plagioclase compositions evolve from high Mg# values and high anorthite contents (An, where An = Ca/(Ca+Na) on a molar basis) towards lower Mg# values and lower An contents with decreasing temperature, respectively. Liquid $Fe^{3+}/\Sigma Fe$ contents increase slightly with decreasing temperature (by ~0.05 over a 100 °C interval), while clinopyroxene $Fe^{3+}/\Sigma Fe$ contents decrease somewhat (by 0.05–0.10 over a similar interval). This divergence in liquid and clinopyroxene $Fe^{3+}/\Sigma Fe$ contents reflects the relative incompatibility of Fe^{3+}, with equilibrium $D^{cpx-liq}_{Fe^{3+}}$ values decreasing from ~0.6 at the liquidus to ~0.4 at 1150 °C in both tholeiitic systems. These values are consistent with a value of 0.453±0.158 reported from (near-)CMAS experiments containing trace Fe (Mallmann & O'Neill, 2009), as well as values estimated from natural clinopyroxene-liquid equilibria in a suite of OIBs that includes the samples considered here (Neave *et al.*, 2024b). Equilibrium $K^{cpx-liq}_{D,Fe^{2+}-Mg}$ values lie in the range 0.23–0.27, and increase slightly with decreasing temperature. While this temperature dependency is captured in the $K^{cpx-liq}_{D,\Sigma Fe-Mg}$ model of Putirka (2008), we note that the $K^{cpx-liq}_{D,Fe^{2+}-Mg}$ values we calculate here (0.23–0.27) are lower than the $K^{cpx-liq}_{D,\Sigma Fe-Mg}$ values estimated from this model (~0.29 at 1250 °C to ~0.27 at 1150 °C). Our calculations thus corroborate recent suggestions by Neave *et al.* (2024b) that true $K^{cpx-liq}_{D,Fe^{2+}-Mg}$ values may lie much closer to those estimated from experiments on mafic alkaline magmas and calc-alkaline basalts (0.24–0.26; Sisson & Grove, 1993; Pilet *et al.*, 2010; Salazar-Naranjo & Vlach, 2023) than the global fit presented by Putirka (2008), at least for our tholeiitic bulk compositions.

Variations in $X_{Fe^{3+}}$ from 0.10 to 0.20 do not significantly affect equilibrium phase proportions calculated for our tholeiitic bulk compositions beyond enhancing the stability of olivine at lower $X_{Fe^{3+}}$ and orthopyroxene at higher $X_{Fe^{3+}}$ (e.g., Figs. 4A and 5A versus 4C and 5C). In contrast, phase compositions are affected by changes in $X_{Fe^{3+}}$, with liquid Mg#, liquid $Fe^{3+}/\Sigma Fe$, clinopyroxene Mg#, and clinopyroxene $Fe^{3+}/\Sigma Fe$ correlating positively with $X_{Fe^{3+}}$. Despite this, $D^{cpx-liq}_{Fe^{3+}}$ and $K^{cpx-liq}_{D,Fe^{2+}-Mg}$ values remain broadly constant at a range of $X_{Fe^{3+}}$. In line with parameterisations describing f_{O_2} as a function of silicate liquid composition (Kress & Carmichael, 1991; Borisov *et al.*, 2018), $X_{Fe^{3+}}$ and liquid $Fe^{3+}/\Sigma Fe$ are closely related to f_{O_2} across the T–$X_{Fe^{3+}}$ conditions investigated, with $X_{Fe^{3+}}$ = 0.1 and 0.2 corresponding to f_{O_2} conditions of ~FMQ−0.5 and ~FMQ+1.0, respectively (Figs. 3A and 3B).

Equilibrium phase proportions calculated for our alkali basalt bulk composition (PI-011) differ from those calculated for our two tholeiitic bulk compositions in that olivine is the liquidus phase and remains stable to low liquid proportions at a range of $X_{Fe^{3+}}$ (Fig. 6), consistent with PI-011 having accumulated mafic phases. Clinopyroxene stability is also enhanced at any given $X_{Fe^{3+}}$ with respect to plagioclase when compared with the two tholeiitic compositions; clinopyroxene joins the crystallising assemblage at temperatures ~40 °C higher than plagioclase in PI-011 but at similar temperatures in the tholeiitic compositions. As for the tholeiitic compositions, clinopyroxene Mg# values, plagioclase An contents and olivine forsterite (Fo, where Fo = Mg/(Mg+Fe^{2+}) on a molar basis) contents decrease steadily with decreasing temperature. Modest (~0.05) increases and decreases in liquid and clinopyroxene $Fe^{3+}/\Sigma Fe$ contents, respectively, with decreasing temperature (from ≥1200 °C to 1120 °C) are of similar magnitudes to those observed in tholeiitic bulk compositions. Above ~1160 °C, the $Fe^{3+}/\Sigma Fe$ content of clinopyroxene is slightly higher than that of liquid, while below ~1160 °C liquid has a higher $Fe^{3+}/\Sigma Fe$ content than clinopyroxene. This crossover in $Fe^{3+}/\Sigma Fe$ contents can be explained by the incompatibility of Fe^{3+} in the crystallising assemblage, including within clinopyroxene, for which equilibrium $D^{cpx-liq}_{Fe^{3+}}$ values are estimated to lie between 0.6 and 0.8; $D^{cpx-liq}_{Fe^{3+}}$ values increase slightly with decreasing temperature before reaching maxima at ~1175 °C, below which they decrease. These values are slightly higher than those calculated for our tholeiitic compositions but are still comparable with the (limited) estimates available from compositionally diverse natural and experimental systems (Mallmann & O'Neill, 2009; Davis & Cottrell, 2021; Neave *et al.*, 2024b). Equilibrium $K^{ol-liq}_{D,Fe^{2+}-Mg}$ values show expected increases from ~0.3 at 1250 °C to ~0.4 at 1100 °C (Toplis, 2005; Saper *et al.*, 2022). Equilibrium $K^{cpx-liq}_{D,Fe^{2+}-Mg}$ trends mirror those in $K^{ol-liq}_{D,Fe^{2+}-Mg}$, increasing from 0.26–0.27 at the clinopyroxene liquidus to 0.30–0.35 at 1100 °C. Although values of 0.30–0.35 at 1100 °C are much higher than those reported from experiments on mafic alkaline systems (0.24–0.25; Pilet *et al.*, 2010; Salazar-Naranjo & Vlach, 2023), values of 0.26–0.27 at 1200 °C—closer to the temperatures at which the experiments of Salazar-Naranjo & Vlach (2023) were performed—are not substantially different. Regardless, temperature appears to have a stronger influence over $K^{cpx-liq}_{D,Fe^{2+}-Mg}$ values in alkalic systems than tholeiitic systems.

As for our tholeiitic bulk compositions, variations in $X_{Fe^{3+}}$ have only a limited impact on equilibrium phase proportions in PI-011 at high liquid proportions that is primarily reflected by a reduction in modal olivine as $X_{Fe^{3+}}$ increases. Phase compositions do however shift as a function of $X_{Fe^{3+}}$, with increases in $X_{Fe^{3+}}$ from 0.15 to 0.35 leading to modest increases in Mg# and Fo of a few mol.% and substantial increases in liquid and

clinopyroxene $Fe^{3+}/\Sigma Fe$ contents of ~0.2. Regardless, $D^{cpx-liq}_{Fe^{3+}}$ and $K^{cpx-liq}_{D,Fe^{2+}-Mg}$ values vary only slightly with $X_{Fe^{3+}}$. In parallel with our tholeiitic bulk compositions, $X_{Fe^{3+}}$ and liquid $Fe^{3+}/\Sigma Fe$ content are closely related to f_{O_2}, with $X_{Fe^{3+}} = 0.15$ and 0.35 corresponding to f_{O_2} conditions of ~FMQ+0.5 and ~FMQ+2.0, respectively (Fig. 3C).

Pseudosection calculations return notably different equilibrium phase proportions for our trachybasaltic-to-tephritic bulk composition (PI-041; Fig. 7) than for the alkali basalt bulk composition discussed above (PI-011). Unexpectedly for an alkalic bulk composition, plagioclase is both the liquidus phase and modally dominant, likely because we used anhydrous models to perform calculations on a moderately hydrous natural system. Some degree of plagioclase accumulation may also have affected the bulk composition. Clinopyroxene is the next-most abundant mineral phase at most temperatures, with the olivine and orthopyroxene being relatively more abundant at low and high $X_{Fe^{3+}}$, respectively. Ilmenite is typically stable below ~1140 °C. Plagioclase An, clinopyroxene Mg# and olivine Fo decrease as functions of temperature at similar rates in PI-041 to in PI-011 and the tholeiitic bulk compositions. However, in contrast with the other bulk compositions, trajectories of liquid and clinopyroxene $Fe^{3+}/\Sigma Fe$ content evolution with decreasing temperature differ greatly at different values of $X_{Fe^{3+}}$. Over the interval ~1150 °C to 1100 °C, both liquid and clinopyroxene $Fe^{3+}/\Sigma Fe$ contents increase by ~0.05 at $X_{Fe^{3+}} = 0.15$, stay broadly constant at $X_{Fe^{3+}} = 0.25$ and diverge at $X_{Fe^{3+}} = 0.35$, whereby liquid $Fe^{3+}/\Sigma Fe$ decreases very slightly and clinopyroxene $Fe^{3+}/\Sigma Fe$ decreases by ~0.1. These differences in $Fe^{3+}/\Sigma Fe$ systematics are reflected in differences in equilibrium $D^{cpx-liq}_{Fe^{3+}}$ values at different $X_{Fe^{3+}}$: $D^{cpx-liq}_{Fe^{3+}}$ values are low at $X_{Fe^{3+}} = 0.15$ (~0.25–0.50) and increase with decreasing temperature but remain broadly constant with decreasing temperature at ~0.5 and ~0.6 at $X_{Fe^{3+}} = 0.25$ and $X_{Fe^{3+}} = 0.35$, respectively. Although calculated $K^{ol-liq}_{D,Fe^{2+}-Mg}$ and $K^{cpx-liq}_{D,Fe^{2+}-Mg}$ values are high (0.35–0.40 and 0.30–0.35, respectively), they are consistent with values calculated at lower temperatures for PI-011, in line with the relatively evolved composition of PI-041 (cf. Toplis, 2005). However, $K^{cpx-liq}_{D,Fe^{2+}-Mg}$ values show a similar dependence on $X_{Fe^{3+}}$ with decreasing temperature to $D^{cpx-liq}_{Fe^{3+}}$ values, with $K^{cpx-liq}_{D,Fe^{2+}-Mg}$ decreasing with decreasing temperature at $X_{Fe^{3+}} = 0.15$, but increasing with decreasing temperature at $X_{Fe^{3+}} = 0.35$. Regardless, more work is required to understand $K^{cpx-liq}_{D,Fe^{2+}-Mg}$ systematics in alkalic magmas given the discord between the experimental observations of Salazar-Naranjo & Vlach (2023) that imply $K^{cpx-liq}_{D,Fe^{2+}-Mg}$ values of ~0.25 in anhydrous tephritic compositions under graphite-saturated (i.e., reducing) conditions and our modelling results that imply higher values of > 0.3 under more naturally relevant f_{O_2} conditions at or above FMQ. Calculations performed at equivalent $X_{Fe^{3+}}$ values return slightly more reducing f_{O_2} conditions for PI-041 than PI-011, with $X_{Fe^{3+}} = 0.15$ corre-

sponding to f_{O_2} conditions evolving from ~FMQ to ~FMQ+0.5 as temperature decreases from 1200 °C to 1100 °C, and $X_{Fe^{3+}} = 0.35$ corresponding to f_{O_2} conditions evolving from ~FMQ+2.0 to ~FMQ+1.5 (Fig. 3D).

The evolution of modelled liquid compositions

The evolution trajectories of modelled liquid compositions (i.e., liquid lines of descent) as functions of $X_{Fe^{3+}}$ are shown in Fig. 8. Liquid lines of descent are shown for modal proportions of liquid that range from 1 to 0.4 (Figs. 4–7), below which differences between fractional and equilibrium crystallisation become increasingly significant (Neave *et al.*, 2019a). Overall, our tholeiitic and alkalic bulk compositions show two different styles of liquid evolution. Tholeiitic compositions are defined by no initial change in SiO_2 and modest increases in alkalis from low initial concentrations (K_2O) < 0.5 wt.%) as Mg# and temperature decrease (Figs. 8A and 8B); our Laki composition shows a sudden increase in SiO_2 at lower temperatures that is associated with the stabilisation of ilmenite. In contrast, alkalic compositions are defined by slight increases in SiO_2 coupled with more substantial increases in alkalis from higher initial concentrations (K_2O > 1 wt.%). Beyond shifting Mg# to higher values, increasing $X_{Fe^{3+}}$ does not have a significant impact on the evolution of SiO_2 in our modelled compositions.

Variation in $X_{Fe^{3+}}$ has a significant impact on the Fe valance systematics of our modelled liquid compositions, which also manifests as differences in modelled f_{O_2} conditions (Figs. 3 and 8C–8F). As anticipated, increasing $X_{Fe^{3+}}$ decreases liquid FeO contents and increases liquid Fe_2O_3 contents. Liquid lines of descent for compositions from the tholeiitic Holuhraun and Laki eruptions broadly overlap. While crystallisation drives up the FeO and Fe_2O_3 content of our modelled tholeiitic liquids, liquid $Fe^{3+}/\Sigma Fe$ contents increase slightly, suggesting that Fe_2O_3 is only marginally more incompatible than FeO during magmatic differentiation. Notably, estimated f_{O_2} conditions remain broadly constant during the evolution of our modelled liquids.

Crystallisation exerts a broadly similar effect on liquid compositions during the evolution of our alkali basalt composition (PI-011) as during the evolution of our tholeiitic compositions. Namely, both FeO and Fe_2O_3 increase down to 1100 °C regardless of $X_{Fe^{3+}}$, with liquid $Fe^{3+}/\Sigma Fe$ increasing slightly and estimated f_{O_2} conditions remaining largely stable. Overall, liquid $Fe^{3+}/\Sigma Fe$ contents increase slightly more for any given drop in temperature than they do for the tholeiitic compositions, suggesting that Fe_2O_3 is relatively more incompatible with respect to FeO in alkalic systems than in tholeiitic systems. A sudden drop in liquid Fe_2O_3 and $Fe^{3+}/\Sigma Fe$ at high $X_{Fe^{3+}}$ (0.35) and low temperatures

can be attributed to the stabilisation of magnetite (Fig. 2C).

In terms of $Fe^{3+}/\Sigma Fe$ contents, calculated liquid lines of descent are more variable for our trachybasaltic-to-tephritic composition (PI-041) than for our alkali basalt composition (PI-011). At low $X_{Fe^{3+}}$ values of 0.15, liquid $Fe^{3+}/\Sigma Fe$ contents increase similarly to how they do during the crystallisation of PI-011. Conversely, at high $X_{Fe^{3+}}$ values of 0.35, liquid $Fe^{3+}/\Sigma Fe$ contents decrease. Variations in $X_{Fe^{3+}}$ thus have a significant effect on the evolution trajectory of trachybasaltic-to-tephritic magmas like PI-041, likely driven by a trade-off between olivine crystallisation at low $X_{Fe^{3+}}$ and magnetite crystallisation at high $X_{Fe^{3+}}$ (Fig. 2D), though differences in clinopyroxene compositions may also play a role.

Modelled clinopyroxene compositions

The evolution trajectories of modelled clinopyroxene compositions (i.e., crystal lines of descent) as functions of $X_{Fe^{3+}}$ are shown in Fig. 9. As for liquid lines of descent, crystal lines of descent are shown for modal proportions of liquid that range from 1 to 0.4. Modelled clinopyroxene compositions are compared with published clinopyroxene compositions from Neave *et al.* (2024b) that were obtained with an EPMA method optimised to return precise clinopyroxene $Fe^{3+}/\Sigma Fe$ contents. These measurements are augmented with an extensive clinopyroxene dataset from Halldórsson *et al.* (2018) in the case of the Holuhraun eruption, partly because the clinopyroxene compositions reported for this eruption by Neave *et al.* (2024b) may have been affected by reductive SO_2 degassing.

Modelled clinopyroxene compositions broadly reproduce the mean Mg#–CaO–Al_2O_3 compositions of clinopyroxene crystals from our tholeiitic bulk compositions (Figs. 9A and 9B). Much of the variability in natural clinopyroxene CaO and Al_2O_3 compositions may thus reflect kinetic processes associated with a combination of disequilibrium crystallisation and sector zone development (Neave *et al.*, 2019a; Ubide *et al.*, 2019; MacDonald *et al.*, 2023). Importantly, the close correspondence between modelled and natural clinopyroxene compositions suggests that the *x*-eos models effectively predict the distribution of quadrilateral and non-quadrilateral components in clinopyroxene crystals from tholeiitic systems. Although $X_{Fe^{3+}}$ has only a minimal effect on modelled clinopyroxene CaO and Al_2O_3 contents it has, unsurprisingly, a major effect on modelled clinopyroxene Fe_2O_3 and $Fe^{3+}/\Sigma Fe$ contents (Figs. 9C and 9D), with mean Fe_2O_3 and $Fe^{3+}/\Sigma Fe$ contents from Holuhraun and Laki best reflected by trends at $X_{Fe^{3+}} \sim 0.15$; some measured clinopyroxene compositions are considerably more enriched in Fe^{3+} than our modelled compositions, though these likely record disequilibrium crystallisation (Neave *et al.*, 2024b).

Modelled clinopyroxene compositions roughly reproduce the Mg#–Al_2O_3 systematics of clinopyroxene crystals from our alkalic bulk compositions (Fig. 9B). However, in contrast with modelled compositions from our tholeiitic bulk compositions, modelled clinopyroxene compositions from our alkalic bulk compositions significantly underestimate observed CaO contents (Fig. 9A). While the offset is merely appreciable for the relatively primitive PI-011 bulk composition (natural crystals contain ∼22 wt.% CaO and modelled crystals contain ∼17–20 wt.%), it is very significant for the relatively evolved PI-041 bulk composition (natural crystals contain ∼22 wt.% CaO while modelled crystals contain ∼10–18 wt.%). These observations suggest that while the x-eos models seem able to reproduce the abundance of Al-bearing non-quadrilateral components (including Ca-Tschermak's component, Esseneite and jadeite; CaTs, Es and Jd) they underestimate the abundance of Ca-rich diopside (Di) and hedenbergite (Hd) components with respect to Ca-poor enstatite (En) and ferrosilite (Fs) components. The most likely explanation for this apparently poor model performance is that modelled liquids and clinopyroxenes are depleted in CaO with respect to what is observed in natural samples because Ca-rich plagioclase is stabilised at higher temperatures in our anhydrous models than in moderately hydrous natural systems, which feature estimated H_2O contents up to ∼1.5 wt% (van Gerve *et al.*, 2024). We tested the plausibility of this explanation by calculating a pseudosection with H_2O varying from 0 to 2 wt.% for the sub-alkaline Holuhraun composition (Supplementary Fig. 1). While H_2O-bearing alkalic melts cannot currently be modelled, precluding examination of the alkalic Pico compositions, our illustrative calculations on a tholeiitic composition demonstrate that the CaO content of near-liquidus clinopyroxene crystals increases with increasing magmatic H_2O (Fig. 10). That is, for any given modal proportion of clinopyroxene, the CaO content of clinopyroxene crystals increases with increasing magmatic H_2O and concomitant decreases in the modal proportion of plagioclase. It is reasonable to consider this model result would also extend to alkalic systems, such that the proposed explanation is plausible. Current clinopyroxene x-eos models may also perform poorly in mafic alkaline systems, because of the relative paucity of experimental observations against which to calibrate such models (cf., Molendijk *et al.*, 2023). It is nonetheless important to note that the discrepancy between high CaO in natural crystals and low CaO in modelled crystal compositions cannot be explained by models being calculated in an equilibrium paradigm and natural crystals growing under disequilibrium conditions—at high degrees of disequilibrium, clinopyroxene crystals incorporate Ca-poor En and Fs at the expense of Ca-rich Di and Hd, creating an opposite trend from what we observe (Mollo *et al.*, 2010; Masotta *et al.*, 2019). Encouragingly, modelled clinopyroxene Fe_2O_3 and $Fe^{3+}/\Sigma Fe$ contents (Figs. 9C and 9D) broadly overlap with those observed

in natural crystals. Specifically, most natural crystals from PI-011 lie between the $X_{Fe^{3+}}$ = 0.15 and $X_{Fe^{3+}}$ = 0.25 trends while most natural crystals from PI-041 lie towards the $X_{Fe^{3+}}$ = 0.35 trend. As for CaO, correspondences in Fe_2O_3 and $Fe^{3+}/\Sigma Fe$ contents between natural and modelled crystals in PI-041 get worse as $X_{Fe^{3+}}$ decreases.

Application to natural systems

Insights into iron-magnesium exchange equilibria

Olivine-liquid equilibria are often summarised and evaluated in terms of $K^{ol-liq}_{D,Fe^{2+}-Mg}$ values that canonically lie close to 0.3 in basaltic systems (Ford *et al.*, 1983) but nonetheless depend on temperature and melt composition in ways described by diverse parameterisations (e.g., Toplis, 2005; Blundy *et al.*, 2020; Saper *et al.*, 2022). Despite their potential utility, similarly comprehensive models are currently unavailable for the evaluation of clinopyroxene-liquid equilibria, likely because of the challenges traditionally associated with determining clinopyroxene $Fe^{3+}/\Sigma Fe$ contents (Neave *et al.*, 2024b); the parameterisations of Wood & Blundy (1997) and Putirka (2008) consider total Fe (i.e., $K^{cpx-liq}_{D,\Sigma Fe-Mg}$ rather than $K^{cpx-liq}_{D,Fe^{2+}-Mg}$ values) and are thus associated with large uncertainties. In their recent evaluation of clinopyroxene-liquid equilibria in natural systems, Neave *et al.* (2024b) argued that true $K^{ol-liq}_{D,Fe^{2+}-Mg}$ values in oceanic basalts may lie closer to values of 0.24–0.26 derived from experiments on mafic alkaline and calc-alkaline magmas (Sisson & Grove, 1993; Pilet *et al.*, 2010; Salazar-Naranjo & Vlach, 2023) than values of ~0.28 estimated from Equation 35 of Putirka (2008). In the absence of targeted experiments, the results of our pseudosection modelling provides us with independent insights into $K^{cpx-liq}_{D,Fe^{2+}-Mg}$ values across a range of primitive magma compositions.

In the regions of our pseudosections where olivine is stable, $K^{ol-liq}_{D,Fe^{2+}-Mg}$ values range from ~0.32 at 1250 °C to ~0.40 at 1100 °C (Figs. 2C and 2D), in line with the convolved effects of temperature and melt composition on $K^{ol-liq}_{D,Fe^{2+}-Mg}$ (Toplis, 2005; Saper *et al.*, 2022); the effect of $X_{Fe^{3+}}$ on $K^{ol-liq}_{D,Fe^{2+}-Mg}$ appears minimal. As described above, $K^{ol-liq}_{D,Fe^{2+}-Mg}$ values vary between tholeiitic and alkalic bulk compositions, and in the case of the latter also vary as a function of $X_{Fe^{3+}}$ (Figs. 2C and 2D).

In our tholeiitic bulk compositions, $K^{cpx-liq}_{D,Fe^{2+}-Mg}$ values increase from ~0.23 at 1190 °C to ~0.27 at 1100 °C. Thus, $K^{cpx-liq}_{D,Fe^{2+}-Mg}$ values follow the same trend of increasing with decreasing temperature as $K^{ol-liq}_{D,Fe^{2+}-Mg}$ values, albeit offset to lower values. Our pseudosection modelling also substantiates the inferences of Neave *et al.* (2024b) that true $K^{cpx-liq}_{D,Fe^{2+}-Mg}$ values in tholeiitic systems (at ~1100 °C) lie closer to the 0.24–0.26 values reported by

Sisson & Grove (1993), Pilet *et al.* (2010) and Salazar-Naranjo & Vlach (2023) than those of ∼0.28 calculated with Equation 35 of Putirka (2008), though values of 0.24–0.26 are still within the considerable ±0.08(1σ) uncertainty of values calculated with the latter (0.27–0.29). It is also notable that these experimentally derived values were obtained from mafic alkaline and calc-alkaline systems; targeted experiments on tholeiitic systems are urgently required.

In our alkalic bulk compositions, $K^{\mathrm{cpx-liq}}_{\mathrm{D,Fe^{2+}-Mg}}$ values increase from ∼0.26–0.28 at 1200 °C to ∼0.30–0.35 at 1100 °C, with lower values in each range being associated with lower $X_{\mathrm{Fe^{3+}}}$ values of 0.15 and higher values with higher $X_{\mathrm{Fe^{3+}}}$ values of 0.35. Different, complex behaviour is observed in PI-041 at low $X_{\mathrm{Fe^{3+}}}$, likely as a consequence of the strong effect of $X_{\mathrm{Fe^{3+}}}$ on modelled clinopyroxene compositions (Fig. 9). Regardless, $K^{\mathrm{cpx-liq}}_{\mathrm{D,Fe^{2+}-Mg}}$ values calculated for our alkalic bulk compositions (0.26–0.35) are appreciably higher than those calculated for our tholeiitic systems (0.23–0.27), especially at low temperatures. They are also, for the most part, lower than the $K^{\mathrm{cpx-liq}}_{\mathrm{D,\Sigma Fe-Mg}}$ values obtained with Equation 35 of Putirka (2008). Paradoxically, $K^{\mathrm{cpx-liq}}_{\mathrm{D,Fe^{2+}-Mg}}$ values from experiments on alkalic systems appear to fit $K^{\mathrm{cpx-liq}}_{\mathrm{D,Fe^{2+}-Mg}}$ values calculated for tholeiitic systems better than those calculated for alkalic systems (∼0.24–0.25 versus ∼0.26–0.35; Pilet *et al.*, 2010; Salazar-Naranjo & Vlach, 2023). However, we believe that sensitivity of $K^{\mathrm{cpx-liq}}_{\mathrm{D,Fe^{2+}-Mg}}$ values to variations in $X_{\mathrm{Fe^{3+}}}$ may provide an explanation. The experiments reported by Pilet *et al.* (2010) and Salazar-Naranjo & Vlach (2023) were largely performed in graphite-saturated conditions fixed at or below ∼FMQ−1.5, conditions considerably more reducing, and commensurately poorer in Fe^{3+}, than those likely to apply in natural systems (FMQ+1 to FMQ+2 or more; Moussallam *et al.*, 2019). In light of this, we revisit the inferences made by Neave *et al.* (2024b) concerning using clinopyroxene-liquid equilibria to estimate magmatic $f_{\mathrm{O_2}}$ conditions in a following section, albeit with the caveat that the x-eos models used may be incompletely calibrated for the compositions investigated.

Insights into ferric iron partitioning

There are currently very few estimates of $D^{\mathrm{cpx-liq}}_{\mathrm{Fe^{3+}}}$ values in magmatic systems. Experimental observations are limited to those from Martian meteorites under reducing conditions (McCanta *et al.*, 2004), simple systems containing only trace Fe (Mallmann & O'Neill, 2009) and peridotitic systems at high pressure (Davis & Cottrell, 2021). As part of their evaluation of clinopyroxene-liquid equilibria in natural ocean island basalts, Neave *et al.* (2024a) described apparent $D^{\mathrm{cpx-liq}}_{\mathrm{Fe^{3+}}}$ values spanning the range 0.2–1.0. However, they argued that the range they observed largely reflected kinetic processes, with much Fe^{3+}

variability arising from a combination of disequilibrium crystallisation and sector zone development generating correlated variability in Al, Ti and Fe^{3+}. That is, they inferred that Al, and ^{IV}Al in particular, placed steric constraints on the incorporation of Fe^{3+}, even if such relationships were only evident because of kinetics, such that true $D_{Fe^{3+}}^{cpx-liq}$ values may instead lie close to their estimated means (∼0.6).

Estimates of $D_{Fe^{3+}}^{cpx-liq}$ values obtained from our pseudosection modelling are presented in Fig. 11. Overall, estimated $D_{Fe^{3+}}^{cpx-liq}$ values are remarkably consistent across wide ranges of $X_{Fe^{3+}}$, bulk composition and clinopyroxene composition. Namely, $D_{Fe^{3+}}^{cpx-liq}$ values calculated for our Holuhraun, Laki and PI-011 bulk compositions define a rough trend with $D_{Fe^{3+}}^{cpx-liq}$ values decreasing from ∼0.7 in Mg# = 0.85 clinopyroxene crystals to ∼0.5 in Mg# = 0.65 clinopyroxene crystals. At high $X_{Fe^{3+}}$, PI-041 returns $D_{Fe^{3+}}^{cpx-liq}$ values consistent with the other compositions, though these deviate to lower $D_{Fe^{3+}}^{cpx-liq}$ values (<0.4) at lower $X_{Fe^{3+}}$, in line with the distinctive clinopyroxene compositions calculated under these conditions (Fig. 9). Our pseudosection modelling thus suggests that clinopyroxene Al and ^{IV}Al contents exert little to no control over equilibrium $D_{Fe^{3+}}^{cpx-liq}$ values (Figs. 11C and 11D), reinforcing the suggestion of Neave *et al.* (2024b) that equilibrium (as opposed to kinetically controlled) $D_{Fe^{3+}}^{cpx-liq}$ values are close to 0.6. Values of 0.453±0.158(1σ) and 0.78±0.30(1σ) reported by Mallmann & O'Neill (2009) and Davis & Cottrell (2021), respectively, are thus broadly representative of basaltic systems. These results also show the importance of considering kinetics when evaluating Fe^{3+} partitioning into clinopyroxene crystals. Nevertheless, that $D_{Fe^{3+}}^{cpx-liq}$ values vary between different bulk and clinopyroxene compositions confirms that melt $Fe^{3+}/\Sigma Fe$ contents and thence f_{O_2} conditions cannot be recovered by assuming that Fe^{3+} partitioning is Henrian, which is unsurprising given the fact that Fe^{3+} is a major rather than trace constituent of magmatic clinopyroxene crystals (McGuire *et al.*, 1989; Neave *et al.*, 2024b).

Estimating magma redox conditions

The $Fe^{3+}/\Sigma Fe$ content of volcanic of glasses can be related to f_{O_2} conditions via (P–)T–X-dependent parameterisations because the amorphous structure of melts (and thus glasses) place no steric constraints on their $Fe^{3+}/\Sigma Fe$ contents. In contrast, clinopyroxene $Fe^{3+}/\Sigma Fe$ contents depend on the structure of the clinopyroxene crystals as well as their composition and prevailing f_{O_2} conditions, preventing the simple parameterisation of f_{O_2} as a function of clinopyroxene compositions and $Fe^{3+}/\Sigma Fe$ contents. However, by calculating pseudosections for specific bulk compositions, it is possible to generate bespoke parameterisations that can relate equilibrium clinopyroxene $Fe^{3+}/\Sigma Fe$ contents to f_{O_2} con-

ditions on a sample-by-sample basis, circumventing the need to account for steric controls over the relative incorporation of Fe^{2+} and Fe^{3+}; steric effects are implicitly accounted for in the thermodynamic models.

Relationships between modelled clinopyroxene $Fe^{3+}/\Sigma Fe$ contents and f_{O_2} expressed as log unit deviations from FMQ (ΔFMQ) are shown in Fig. 12A. To ensure that modelled clinopyroxene compositions feasibly reflect measured compositions of natural crystals, we only considered near-liquidus compositions from regions of the pseudosections associated with $\leq$5% modal clinopyroxene. Importantly, f_{O_2} does not vary much at any given $Fe^{3+}/\Sigma Fe$ content for near-liquidus clinopyroxene crystals in any given bulk composition. However, it is striking that f_{O_2} can vary by a log unit or more at a fixed clinopyroxene $Fe^{3+}/\Sigma Fe$ content between different bulk compositions (Fig. 12A; Weller *et al.*, 2024). In general, the more evolved the bulk composition, the higher the f_{O_2} at any fixed clinopyroxene $Fe^{3+}/\Sigma Fe$ content, though it is notable that the topology of the clinopyroxene $Fe^{3+}/\Sigma Fe$–f_{O_2} relationship is substantially different for PI-041 than for the other three bulk compositions, reflecting the greater range in modelled clinopyroxene compositions generated as a function $X_{Fe^{3+}}$ for this composition (Fig. 9). Results from PI-041 are nevertheless broadly coherent with those from the other bulk compositions when clinopyroxene $Fe^{3+}/\Sigma Fe$ contents exceed ~0.1, which encompasses the majority of natural compositions (Fig. 9D).

By parameterising relationships between f_{O_2} conditions and clinopyroxene $Fe^{3+}/\Sigma Fe$ contents with the polynomial fits shown in Fig. 12A, we estimated magmatic f_{O_2} conditions from clinopyroxene $Fe^{3+}/\Sigma Fe$ contents on a composition-by-composition basis. We stress that these fits are specific to the pseudosections from which they were derived (i.e., the specific combination of bulk composition and x-eos models used) and cannot be used to relate clinopyroxene $Fe^{3+}/\Sigma Fe$ contents to f_{O_2} conditions more generally. Natural clinopyroxene compositions were first filtered for equilibrium with liquid compositions calculated from the pseudosection modelling. We did this by identifying natural clinopyroxene compositions feasibly in equilibrium with modelled liquid compositions in equilibrium with the clinopyroxene compositions shown in Fig. 12A. We achieved this by excluding natural clinopyroxene compositions that returned $K^{cpx-liq}_{D,Fe^{2+}-Mg}$ values deviating by more than 0.03 when paired with any given modelled liquid at any given $X_{Fe^{3+}}$. This step ensured that the parameterisations shown in Fig. 12A were only applied to natural clinopyroxene compositions that could have feasibly grown from the liquids produced by our pseudosection modelling. We used a threshold of $\pm$0.03 for selecting equilibrium clinopyroxene-liquid pairs because it is conservative with respect to uncertainties in analogous but well understood $K^{ol-liq}_{D,Fe^{2+}-Mg}$ values ($\pm$0.02; Toplis, 2005; Blundy *et al.*, 2020). This uncertainty of $\pm$0.03 is

significantly lower the $\pm 0.08 (1\sigma)$ uncertainty associated with $K^{\text{cpx}-\text{liq}}_{\text{D},\Sigma\text{Fe}-\text{Mg}}$ values calculated with Equation 35 Putirka (2008) that are compromised by ignoring the presence of Fe^{3+}; we posit that $K^{\text{cpx}-\text{liq}}_{\text{D},Fe^{2+}-\text{Mg}}$ values should be more precisely quantifiable than $K^{\text{cpx}-\text{liq}}_{\text{D},\Sigma\text{Fe}-\text{Mg}}$ values when both clinopyroxene and liquid $Fe^{3+}/\Sigma Fe$ contents are known. We also suggest $K^{\text{cpx}-\text{liq}}_{\text{D},\Sigma\text{Fe}-\text{Mg}}$ has been repeatedly identified as a poor discriminator of clinopyroxene-liquid equilibrium with respect to, for example, DiHd and EnFs component equilibria at least in part because of the uncertainties inherent with not evaluating the role of Fe^{3+} (Mollo *et al.*, 2013; Wieser *et al.*, 2023; MacDonald *et al.*, 2023). Importantly, the results of our pseudosection modelling also highlight that $K^{\text{cpx}-\text{liq}}_{\text{D},Fe^{2+}-\text{Mg}}$ values depend not only on temperature as described by Putirka (2008), but also on bulk composition, with $K^{\text{cpx}-\text{liq}}_{\text{D},Fe^{2+}-\text{Mg}}$ values associated with alkalic bulk compositions being appreciably higher than those associated with tholeiitic bulk compositions. Thus, the $K^{\text{cpx}-\text{liq}}_{\text{D},Fe^{2+}-\text{Mg}}$ values used to evaluate equilibrium need to be tailored to the P–T–X conditions of interest. Nevertheless, we note that imposing a fixed $K^{\text{cpx}-\text{liq}}_{\text{D},Fe^{2+}-\text{Mg}}$ value of 0.25 based on experimental observations from Salazar-Naranjo & Vlach (2023) does not change our results significantly: eventual estimates of f_{O_2} for our alkalic samples increase by $\sim$0.2 while those for our tholeiitic samples remain unchanged.

After filtering for equilibrium, f_{O_2} conditions were inferred from natural clinopyroxene compositions on a composition-by-composition basis using the relevant parameterisation shown in Fig. 12A. Estimated f_{O_2} conditions are shown in Fig. 12B. Because the fitted relationships between f_{O_2} and clinopyroxene $Fe^{3+}/\Sigma Fe$ are decidedly non-linear, we report our results as median f_{O_2} conditions and interquartile ranges (IQRs). We also report the evaluations of Fe^{2+}–Mg equilibrium used to filter natural clinopyroxene compositions in Figs. 12C–12F. Equilibrium clinopyroxene–liquid pairs were found for both of the tholeiitic systems investigated (Holuhraun and Laki; Figs. 12C–12E), while equilibrium pairs were only found for one of the alkalic systems considered (PI-041; Fig. 12F); no equilibrium pairs were identified for PI-011, likely because this composition has accumulated mafic phases. Equilibrium $K^{\text{cpx}-\text{liq}}_{\text{D},Fe^{2+}-\text{Mg}}$ values were estimated to lie close to 0.24 for the tholeiitic compositions and close to 0.30 for the alkalic composition (PI-041).

Clinopyroxene compositions from the Holuhraun eruption reported by Neave *et al.* (2024b) return a median f_{O_2} of FMQ−1.2 (IQR = FMQ−1.4 to FMQ−0.9; Fig. 12B). These values suggest a reducing environment with respect to those derived from melt S systematics that favour more oxidising pre-eruptive f_{O_2} conditions of FMQ+0.5 (Bali *et al.*, 2018). Nevertheless, these values agree with the observations of Neave *et al.* (2024b), largely on account on being based on similar $K^{\text{cpx}-\text{liq}}_{\text{D},Fe^{2+}-\text{Mg}}$ values. We thus agree the suggestion of Neave *et al.* (2024b) that the small, tephra-hosted crystals they measured grew

from liquids that had experienced syn-eruptive reduction as a result of SO_2 degassing (e.g., Moussallam *et al.*, 2016). As such we suggest that the clinopyroxene $Fe^{3+}/\Sigma Fe$ content of these crystals reflects a true f_{O_2}, but that this f_{O_2} corresponds to a brief snapshot in the late-stage evolution of the system rather than the f_{O_2} conditions that prevailed at depth. In contrast, clinopyroxene compositions reported by Halldórsson *et al.* (2018) return a median f_{O_2} of FMQ (IQR = FMQ−0.8 to FMQ+0.4; Fig. 12B), comfortably within uncertainty of the ∼FMQ+0.5 value estimated by (Bali *et al.*, 2018), and in line with recalculated values for the Reykjanes Ridge (FMQ−0.3 to FMQ; Shorttle, 2015; Novella *et al.*, 2020). We speculate that the tail to more reducing conditions may reflect similar degassing processes to those inferred from the compositions reported by Neave *et al.* (2024b).

Clinopyroxene compositions from the Laki eruption reported by Neave *et al.* (2024b) return a median f_{O_2} of FMQ+0.6 (IQR = FMQ+0.3 to FMQ+1.2; Fig. 12B). These values are wholly consistent with pre-eruptive f_{O_2} conditions estimated from Fe-XANES spectroscopy performed on olivine-hosted melt inclusions (∼FMQ+0.7; Hartley *et al.*, 2017). Overall, our findings from the Laki eruption suggest that clinopyroxene $Fe^{3+}/\Sigma Fe$ contents derived from crystals or crystal zones that formed shortly before eruption but before any significant SO_2 degassing can provide faithful records of magmatic f_{O_2} conditions, at least for tholeiitic compositions.

Clinopyroxene compositions in sample PI-041 from Pico reported by Neave *et al.* (2024b) return a median f_{O_2} of FMQ+1.1 (IQR = FMQ+0.6 to FMQ+1.6; Fig. 12B). While these f_{O_2} conditions are relatively oxidised when compared with those from MORBs that hover around FMQ (e.g., Cottrell *et al.*, 2022) they are relatively reduced when compared with those estimated for many OIBs, including those with similar geochemical affinities to the Azores (≥FMQ+2; Moussallam *et al.*, 2019; Taracsák *et al.*, 2022; Nicklas *et al.*, 2022b). These conditions also contrast with those recently suggested by Neave *et al.* (2024b) based on the same clinopyroxene compositions we discuss here (≥FMQ+2.5). Neave *et al.* (2024b) based their f_{O_2} estimation on the assumption that $K^{cpx-liq}_{D,Fe^{2+}-Mg}$ values in mafic alkali magmas are not only similar to those in tholeiitic magmas but also to those inferred from experiments on mafic alkali magmas (Pilet *et al.*, 2010; Salazar-Naranjo & Vlach, 2023) and thus lie close to 0.24. As discussed above, our pseudosection modelling instead suggests that $K^{cpx-liq}_{D,Fe^{2+}-Mg}$ values in moderately oxidising alkalic bulk compositions (i.e., natural systems rather than graphite-buffered experimental systems) could be much higher, with equilibrium clinopyroxene-liquid pairs in trachybasaltic-to-tephritic PI-041 being associated with $K^{cpx-liq}_{D,Fe^{2+}-Mg}$ values around 0.30. However, filtering equilibrium clinopyroxene compositions with a fixed $K^{cpx-liq}_{D,Fe^{2+}-Mg}$ value of 0.24 from Salazar-Naranjo &

Vlach (2023) only increases median f_{O_2} estimates to FMQ+1.3 from FMQ+1.1, implying that vagaries in true $K^{cpx-liq}_{D,Fe^{2+}-Mg}$ values cannot account for the apparently low f_{O_2} conditions we estimate for our PI-041. Conversely, we suggest that syn-eruptive SO_2 degassing may have reduced natural PI-041 liquids in a similar way to how it affected the Holuhraun liquids discussed above. For example, most of the equilibrium pairs we identify are associated with lower Mg# clinopyroxene compositions and lower $Fe^{3+}/\Sigma Fe$ contents (Fig. 12). The corollary to this is that the higher Mg# clinopyroxene compositions for which we do not find equilibrium pairs may reflect crystallisation under disequilibrium conditions (e.g., Ubide *et al.*, 2019; Di Fiore *et al.*, 2021), an inference consistent with their location within rapidly grown microcrysts rather than macrocryst rims (Fig. 12D; Neave *et al.*, 2024b). Moreover, our pseudosection modelling approach can only recover f_{O_2} conditions during the last equilibration between liquid and clinopyroxene compositions within the modelled bulk composition. While macrocryst cores may have grown under more oxidising conditions prior to the formation of rims and microcrysts, our current approach cannot recover earlier equilibration events such as these. Indeed, comparisons with the parameterisation for the relatively primitive PI-011 composition suggest that clinopyroxene core $Fe^{3+}/\Sigma Fe$ contents of ∼0.3 could potentially indicate f_{O_2} conditions close to FMQ+2 (Fig. 12A).

Caveats and future directions

Our results suggest that pseudosection modelling can, in principle, provide new ways to relate phase compositions, and clinopyroxene $Fe^{3+}/\Sigma Fe$ contents in particular, to magmatic f_{O_2} conditions. Moreover, they highlight the sensitivity of relationships between clinopyroxene $Fe^{3+}/\Sigma Fe$ contents and f_{O_2} conditions to P–T–X conditions. They also underline how criteria used to identify mineral-liquid equilibrium such as $K^{cpx-liq}_{D,Fe^{2+}-Mg}$ values are also closely tied to P–T–X conditions, with $K^{cpx-liq}_{D,Fe^{2+}-Mg}$ potentially being higher than suggested in alkalic bulk compositions, at least under some circumstances. Nonetheless, there are some important caveats to our approach that reveal directions for future work.

Our first and most important caveat is that the effective application of our approach still depends on understanding the petrographic and petrological contexts of the clinopyroxene analyses being used to estimate f_{O_2} conditions. For example, the two suites of clinopyroxene compositions we consider from the Holuhraun eruption return median f_{O_2} conditions more than a log unit apart. While this discrepancy might initially be ascribed to poor model performance or poor analyses in one or both of the datasets, further investigation shows how it can be reconciled when the histories of different clinopyroxene suites are taken into account; small tephra-hosted clinopyroxene crystals analysed by Neave

et al. (2024b) grew after some degree of reductive SO_2 degassing, while larger and mostly lava-hosted crystals analysed by Halldórsson *et al.* (2018) formed prior to reductive SO_2 degassing. Likewise, the failure to identify any equilibrium clinopyroxene-liquid pairs from PI-011 can be explained by its bulk composition incorporating accumulated mafic minerals and thus not constituting a true magmatic liquid. Degassing may have also played an important role creating the only moderately oxidising f_{O_2} conditions recorded by equilibrium clinopyroxene crystals in PI-041.

A further key caveat associated with thermodynamic modelling of any kind concerns whether the models being used are sufficiently well calibrated under the conditions of interest. While thermodynamic models have some predictive power beyond their immediate calibration ranges, their performance is still compromised in systems that have seen little experimental investigation. The expansion of benchmarked x-eos liquid models into basaltic and then alkaline compositional fields provides encouragement that our pseudosection models are sufficiently well founded (Green *et al.*, 2016; Weller *et al.*, 2024). The offset between natural and modelled clinopyroxene compositions in our alkalic bulk compositions is nevertheless striking, especially in terms of the apparent underestimation of CaO, and thus DiHd component, contents (Fig. 9A). Although overestimating the plagioclase stability due to the anhydrous model system being compared with a moderately hydrous natural system is probably a key cause of this discrepancy, the relative paucity of well-characterised clinopyroxene compositions in a range of alkalic experimental systems against which to benchmark clinopyroxene x-eos models provided by Weller *et al.* (2024) (that reflect an evolution of the models presented by Green *et al.* (2012), Jennings & Holland (2015) and Holland *et al.* (2018)) may also play an important role. In contrast, modelled clinopyroxene compositions do a good job of reproducing natural compositions in our tholeiitic systems, reflecting the greater abundance of experimental observations in this compositional space with which to calibrate and benchmark models (e.g., Holland *et al.*, 2018).

Our modelling does not account for the presence of magmatic H_2O due to the current absence of x-eos models for hydrous alkaline systems, which is a key target for future model development (Weller *et al.*, 2024). It is nevertheless important to note that ignoring H_2O is likely to have the biggest impact on the pseudosections calculated for our alkalic bulk compositions that contain up to ~1.5 wt.% (van Gerve *et al.*, 2024), though tholeiitic bulk compositions still contain non-negligible H_2O contents up to ~0.7 wt.% (Hartley *et al.*, 2014). The main impact of modelling moderately hydrous systems with an anhydrous model is that the stability of plagioclase will likely be overestimated (Almeev *et al.*, 2012). This is probably why clinopyroxene CaO contents are strongly underestimated in our

models of alkalic systems where the crystallisation of CaO-rich plagioclase is often observed to be suppressed with respect to clinopyroxene crystallisation in hydrous natural systems, as demonstrated by illustrative calculations using H_2O sensitive models in a tholeiitic system (Fig 10).

Our magma redox estimates obtained via pseudosection modelling are variably robust. Pre-eruptive f_{O_2} estimates of FMQ for the Holuhraun eruption to FMQ+0.7 for the Laki eruption agree with prior estimates and are based on models that reproduce natural compositions well. In contrast, a pre-eruptive f_{O_2} estimate of FMQ+1.1 for sample PI-041 from Pico is less oxidising than expected based on prior observations (Neave *et al.*, 2024b). It is also based on models that do not fully reproduce natural compositions, though is also likely to compromised by syn-eruptive reductive degassing of SO_2. Regardless, our estimates of magmatic f_{O_2} conditions from the Azores are less certain than those from Iceland. Future work in two key areas should improve our ability to estimate f_{O_2} conditions from clinopyroxene crystals in alkalic systems. Firstly, incorporating H_2O into pseudosection modelling of alkalic systems will address outstanding uncertainties around the impact of over-stabilising plagioclase on equilibrium clinopyroxene compositions. Secondly, performing new, targetted experiments will allow us to explore how variations in $X_{Fe^{3+}}$ affect clinopyroxene-liquid equilibria and clinopyroxene $Fe^{3+}/\Sigma Fe$ contents in a range of OIB compositions.

Conclusions

By performing pseudosection modelling we parameterised relationships between clinopyroxene $Fe^{3+}/\Sigma Fe$ contents and f_{O_2} conditions for bulk compositions associated with four natural OIB samples from Iceland and the Azores. Using these parameterisations and newly gained insights into Fe^{2+}–Mg exchange equilibria between clinopyroxene crystals and their host liquids we estimated magmatic f_{O_2} conditions from clinopyroxene $Fe^{3+}/\Sigma Fe$ contents in the natural samples. Clinopyroxene crystals in tholeiitic basalts from Iceland record magmatic f_{O_2} conditions of ∼FMQ to ∼FMQ+0.6 that are wholly consistent with previously reported values from the samples in question and, in line with prior assessments (e.g., Shorttle, 2015; Hartley *et al.*, 2017; Bali *et al.*, 2018; Neave *et al.*, 2024b), confirming that Icelandic tholeiites evolve under f_{O_2} conditions similar to or very slightly more oxidised than those experienced by MORBs (Cottrell *et al.*, 2022). Importantly, some small tephra-hosted crystals from the Holuhraun eruption record considerably more reducing conditions of FMQ−1.2 indicating that even mineral-based archives of magma redox conditions can be compromised by late stage reduction by SO_2 degassing. Clinopyroxene

crystals in trachybasalt-to-tephrite from Pico Island in the Azores record more oxidising conditions of ∼FMQ+1.1, qualitatively consistent with relatively oxidising conditions reported from OIBs containing recycled material in their mantle sources, but nonetheless significantly less oxidising than the most oxidised conditions reported from largely analogous systems like the Canary Islands (Moussallam *et al.*, 2019; Brounce *et al.*, 2022). Importantly, these values are much less than the FMQ+2.5 recently reported from the same samples by Neave *et al.* (2024b), though it is also likely that they have been compromised reductive SO_2 degassing on liquid compositions – the FMQ+1.1 for Pico should be viewed as a minimum rather than a maximum.

Overall, our findings show that pseudosection modelling can successfully provide a way to circumvent challenges imposed by steric effects when relating clinopyroxene $Fe^{3+}/\Sigma Fe$ contents with magmatic f_{O_2} conditions. However, further work is required to calibrate and benchmark clinopyroxene x-eos models in the composition space occupied by mafic alkaline magmas, something than can only realistically be attempted following a targeted experimental campaign to this end. Regardless, expanding recently developed x-eos models into hydrous alkalic systems will likely lead to improvements in model performance in moderately hydrous OIB settings like the Azores. When combined with the increasing ease of calculating pseudosections in MAGEMin Riel *et al.* (2022) these developments will continue to enhance our ability to integrate thermodynamic modelling with observations from natural samples to investigate the redox evolution of magmatic systems.

Funding

This work was supported by a NERC Independent Research Fellowship (NE/T011106/1) and a Royal Society Research Grant (RGS\R1\201344) to DAN. CRS and OMW were supported by a UK Research and Innovation Future Leaders Fellowship (MR/V02292X/1).

Acknowledgements

Data availability

This manuscript contains no new data or models. All calculations were performed using published data and models that are cited where relevant throughout the manuscript.

References

Almeev, R. R., F. Holtz, J. Koepke, & F. Parat (2012), Experimental calibration of the effect of H_2O on plagioclase crystallization in basaltic melt at 200 MPa, *American Mineralogist*, 97, 1234–1240, doi:10.1016/j.chemgeo.2008.04.009.

Bali, E., M. E. Hartley, S. A. Halldórsson, G. H. Gudfinnsson, & S. Jakobsson (2018), Melt inclusion constraints on volatile systematics and degassing history of the 2014–2015 Holuhraun eruption, Iceland, *Contributions to Mineralogy and Petrology*, 173, 9, doi:10.1007/s00410-017-1434-1.

Blundy, J. D., E. Melekhova, L. Ziberna, M. C. S. Humphreys, V. Cerantolo, R. A. Brooker, C. A. McCammon, M. Pichavant, & P. Ulmer (2020), Effect of redox on Fe-Mg-Mn exchange between olivine and melt and an oxybarometer for basalts, *Contributions to Mineralogy and Petrology*, 7, 103, doi:10.1007/s00410-020-01736-7.

Borisov, A., H. Behrens, & F. Holtz (2018), Ferric/ferrous ratio in silicate melts: a new model for 1 atm data with special emphasis on the effects of melt composition, *Contributions to Mineralogy and Petrology*, 173(12), 98, doi:10.1007/s00410-018-1524-8.

Brounce, M., E. Stolper, & J. Eiler (2017), Redox variations in Mauna Kea lavas, the oxygen fugacity of the Hawaiian plume, and the role of volcanic gases in Earth's oxygenation, *Proceedings of the National Academy of Sciences*, 114(34), 8997–9002, doi:10.1073/pnas.1619527114.

Brounce, M., E. Cottrell, & K. A. Kelley (2019), The redox budget of the Mariana subduction zone, *Earth and Planetary Science Letters*, 528, 115,859, doi:10.1016/j.epsl.2019.115859.

Brounce, M., E. Stolper, & J. Eiler (2022), The mantle source of basalts from Reunion Island is not more oxidized than the MORB source mantle, *Contributions to Mineralogy and Petrology*, 177(1), 7, doi:10.1007/s00410-021-01870-w.

Burgisser, A., & B. Scaillet (2007), Redox evolution of a degassing magma rising to the surface, *Nature*, 445(7124), 194–197, doi:10.1038/nature05509.

Canil, D., & H. S. C. O'Neill (1996), Distribution of Ferric Iron in some Upper-Mantle Assemblages, *Journal of Petrology*, 37(3), 609–635, doi:10.1093/petrology/37.3.609.

Carmichael, I. S. E. (1991), The redox states of basic and silicic magmas: a reflection of their source regions?, *Contributions to Mineralogy and Petrology*, 106(2), 129–141, doi:10.1007/BF00306429.

Chicchi, L., L. Bindi, D. Fanelli, & S. Tommasini (2023), Frontiers of thermobarometry: GAIA, a novel Deep Learning-based tool for volcano plumbing systems, *Earth and Planetary Science Letters*, 620, 118,352, doi:10.1016/j.epsl.2023.118352.

Cottrell, E., S. K. Birner, M. Brounce, F. A. Davis, L. E. Waters, & K. A. Kelley (2022), Oxygen Fugacity Across Tectonic Settings, in Magma Redox Geochimistry, Geophysical Monograph 266, edited by R. Moretti & D. Neuville, pp. 33–61, John Wiley & Sons, Inc., doi:10.1002/9781119473206.ch3.

Davis, F. A., & E. Cottrell (2021), Partitioning of Fe_2O_3 in peridotite partial melting experiments over a range of oxygen fugacities elucidates ferric iron systematics in mid-ocean ridge basalts and ferric iron content of the upper mantle, *Contributions to Mineralogy and Petrology*, 176(9), 67, doi:10.1007/s00410-021-01823-3.

Di Fiore, F., S. Mollo, A. Vona, A. MacDonald, T. Ubide, M. Nazzari, C. Romano, & P. Scarlato (2021), Kinetic partitioning of major and trace cations between clinopyroxene and phonotephritic melt under convective stirring conditions: New insights into clinopyroxene sector zoning and concentric zoning, *Chemical Geology*, 584, 120,531, doi:10.1016/j.chemgeo.2021.120531.

Evans, K. A., & A. G. Tomkins (2011), The relationship between subduction zone redox budget and arc magma fertility, *Earth and Planetary Science Letters*, 308(3-4), 401–409, doi:10.1016/j.epsl.2011.06.009.

Evans, K. A., & A. G. Tomkins (2022), Redox Variables and Mechanisms in Subduction Magmatism and Volcanism, in Geophysical Monograph Series, edited by R. Moretti & D. R. Neuville, 1 ed., pp. 63–91, Wiley, doi:10.1002/9781119473206.ch4.

Feig, S. T., J. Koepke, & J. E. Snow (2010), Effect of oxygen fugacity and water on phase equilibria of a hydrous tholeiitic basalt, *Contributions to Mineralogy and Petrology*, 160(4), 551–568, doi:10.1007/s00410-010-0493-3.

Ford, C. E., D. G. Russell, J. A. Craven, & M. R. Fisk (1983), Olivine-liquid equilibria: Temperature, pressure and composition dependence of the crystal/liquid cation partition coefficients for Mg , Fe^{2+}, Ca and Mn, *Journal of Petrology*, 24, 256–265.

Frost, B. R. (1991), Introduction to oxygen fugacity and its petrologic importance, *Reviews in Mineralogy and Geochemistry*, 25, 1–9.

Gaetani, G. A. (2016), The Behavior of Fe^{3+}/Fe During Partial Melting of Spinel Lherzolite, *Geochimica et Cosmochimica Acta*, 185, 64–77, doi:10.1016/j.gca.2016.03.019.

Green, E. C. R., T. J. B. Holland, R. Powell, & R. W. White (2012), Garnet and spinel lherzolite assemblages in $MgO–Al_2O_3–SiO_2$ and $CaO–MgO–Al_2O_3–SiO_2$: Thermodynamic models and an experimental conflict, *Journal of Metamorphic Geology*, 30(6), 561–577, doi:10.1111/j.1525-1314.2012.00981.x.

Green, E. C. R., R. W. White, J. F. A. Diener, R. Powell, T. J. B. Holland, & R. M. Palin (2016), Activity-composition relations for the calculation of partial melting equilibria in metabasic rocks, *Journal of Metamorphic Geology*, 34, 845–869, doi:10.1111/jmg.12211.

Halldórsson, S. A., E. Bali, M. E. Hartley, D. A. Neave, D. W. Peate, G. H. GuÃřfinnsson, I. N. Bindeman, & M. J. Whitehouse (2018), Petrology and geochemistry of the 2014–2015 Holuhraun eruption, central Iceland: compositional and mineralogical characteristics, temporal variability and magma storage, *Contributions to Mineralogy and Petrology*, 173, 64, doi:10.1007/s00410-018-1487-9.

Hartley, M. E., J. Maclennan, M. Edmonds, & T. Thordarson (2014), Reconstructing the deep CO2 degassing behaviour of large basaltic fissure eruptions, *Earth and Planetary Science Letters*, 393, 120–131, doi:10.1016/j.epsl.2014.02.031.

Hartley, M. E., O. Shorttle, J. Maclennan, Y. Moussallam, & M. Edmonds (2017), Olivine-hosted melt inclusions as an archive of redox heterogeneity in magmatic systems, *Earth and Planetary Science Letters*, 479, 192–205, doi:10.1016/j.epsl.2017.09.029.

Helz, R. T., E. Cottrell, M. N. Brounce, & K. A. Kelley (2017), Olivine-Melt Relationships and Syneruptive Redox Variations in the 1959 Eruption of Kīlauea Volcano as Revealed by XANES, *Journal of Volcanology and Geothermal Research*, 333-334, 1–14, doi:10.1016/j.jvolgeores.2016.12.006.

Holland, H. D. (2002), Volcanic gases, black smokers, and the great oxidation event, *Geochimica et Cosmochimica Acta*, 66(21), 3811–3826, doi:10.1016/S0016-7037(02)00950-X.

Holland, T. J. B., & R. Powell (2011), An improved and extended internally consistent thermodynamic dataset for phases of petrological interest, involving a new equation of state for solids, *Journal of Metamorphic Geology*, 29(3), 333–383, doi:10.1111/j.1525-1314.2010.00923.x.

Holland, T. J. B., E. C. R. Green, & R. Powell (2018), Melting of peridotites through to granites: a simple thermodynamic model in the system KNCFMASHTOCr, *Journal of Petrology*, 59(5), 881–900, doi:10.1093/petrology/egy048.

Holland, T. J. B., E. C. R. Green, & R. Powell (2022), A thermodynamic model

964 for feldspars in $KAlSi_3O_8$-$NaAlSi_3O_8$-$CaAl_2Si_2O_8$ for mineral equilibrium calculations,
965 *Journal of Metamorphic Geology*, 40(4), 587–600, doi:10.1111/jmg.12639.

966 Hughes, E. C., S. Law, G. Kilgour, J. D. Blundy, & H. M. Mader (2023), Storage, evolution,
967 and mixing in basaltic eruptions from around the Okataina Volcanic Centre, Taupō
968 Volcanic Zone, Aotearoa New Zealand, *Journal of Volcanology and Geothermal Research*,
969 434, 107,715, doi:10.1016/j.jvolgeores.2022.107715.

970 Jennings, E. S., & T. J. B. Holland (2015), A simple thermodynamic model for melting
971 of peridotite in the system NCFMASOCr, *Journal of Petrology*, pp. 1–24, doi:10.1093/
972 petrology/egv020.

973 Jugo, P. J. (2009), Sulfur content at sulfide saturation in oxidized magmas, *Geology*, 37(5),
974 415–418, doi:10.1130/G25527A.1.

975 Kress, V. C., & I. S. E. Carmichael (1991), The compressibility of silicate liquids containing
976 Fe_2O_3 and the effect of composition, temperature, oxygen fugacity and pressure on
977 their redox states, *Contributions to Mineralogy and Petrology*, 108(1-2), 82–92, doi:
978 10.1007/BF00307328.

979 Luth, R. W., & D. Canil (1993), Ferric iron in mantle-derived pyroxenes and a new oxy-
980 barometer for the mantle, *Contributions to Mineralogy and Petrology*, 113(2), 236–248,
981 doi:10.1007/BF00283231.

982 MacDonald, A., T. Ubide, S. Mollo, A. Pontesilli, & M. Masotta (2023), The Influence
983 of Undercooling and Sector Zoning on Clinopyroxene–Melt Equilibrium and Thermo-
984 barometry, *Journal of Petrology*, 64(10), egad074, doi:10.1093/petrology/egad074.

985 Mallmann, G., & H. S. C. O'Neill (2009), The crystal/melt partitioning of V during mantle
986 melting as a function of oxygen fugacity compared with some other elements (Al, P,
987 Ca, Sc, Ti, Cr, Fe, Ga, Y, Zr and Nb), *Journal of Petrology*, 50(9), 1765–1794, doi:
988 10.1093/petrology/egp053.

989 Masotta, M., A. Pontesilli, S. Mollo, P. Armienti, T. Ubide, M. Nazzari, & P. Scarlato
990 (2019), The role of undercooling during clinopyroxene growth in trachybasaltic magmas:
991 Insights on magma decompression and cooling at Mt. Etna volcano, *Geochimica et*
992 *Cosmochimica Acta*, doi:10.1016/j.gca.2019.10.009, publisher: Elsevier Ltd.

993 McCanta, M. C., M. D. Dyar, M. J. Rutherford, & J. S. Delaney (2004), Iron partitioning
994 between basaltic melts and clinopyroxene as a function of oxygen fugacity, *American*
995 *Mineralogist*, 89(11-12), 1685–1693, doi:10.2138/am-2004-11-1214.

McGuire, A. V., M. D. Dyar, & K. A. Ward (1989), Neglected Fe^{3+}/Fe^{2+} ratios – a study of Fe^{3+} content of megacrysts from alkali basalts, *Geology*, 17(8), 687–690, doi:10.1130/0091-7613(1989)017<0687:NFFRAS>2.3.CO.

Molendijk, S. M., O. Namur, P. R. Mason, B. Dubacq, B. Smets, D. A. Neave, & B. Charlier (2023), Trace element partitioning in silica-undersaturated alkaline magmatic systems, *Geochimica et Cosmochimica Acta*, 346, 29–53, doi:10.1016/j.gca.2023.01.025.

Mollo, S., P. Del Gaudio, G. Ventura, G. Iezzi, & P. Scarlato (2010), Dependence of clinopyroxene composition on cooling rate in basaltic magmas: Implications for thermobarometry, *Lithos*, 118(3-4), 302–312, doi:10.1016/j.lithos.2010.05.006.

Mollo, S., K. D. Putirka, V. Misiti, M. Soligo, & P. Scarlato (2013), A new test for equilibrium based on clinopyroxene-melt pairs: Clues on the solidification temperatures of Etnean alkaline melts at post-eruptive conditions, *Chemical Geology*, 352, 92–100, doi:10.1016/j.chemgeo.2013.05.026.

Morimoto, N., J. Fabries, A. K. Ferguson, I. V. Ginzburg, M. Ross, F. A. Seifert, J. Zussman, K. Aoki, & G. Gottardi (1988), Nomenclature of pyroxenes, *American Mineralogist*, 73, 1123–1133, doi:10.1007/BF01226262.

Moussallam, Y., C. Oppenheimer, B. Scaillet, F. Gaillard, P. Kyle, N. Peters, M. E. Hartley, K. Berlo, & A. Donovan (2014), Tracking the changing oxidation state of Erebus magmas, from mantle to surface, driven by magma ascent and degassing, *Earth and Planetary Science Letters*, 393, 200–209, doi:10.1016/j.epsl.2014.02.055.

Moussallam, Y., Y. Morizet, & F. Gaillard (2016), H_2O–CO_2 solubility in low SiO_2-melts and the unique mode of kimberlite degassing and emplacement, *Earth and Planetary Science Letters*, 447, 151–160, doi:10.1016/j.epsl.2016.04.037.

Moussallam, Y., M.-A. Longpré, C. A. McCammon, A. Gómez-Ulla, E. F. Rose-Koga, B. Scaillet, N. Peters, E. Gennaro, R. Paris, & C. Oppenheimer (2019), Mantle plumes are oxidised, *Earth and Planetary Science Letters*, 527, 115,798, doi:10.1016/j.epsl.2019.115798.

Neave, D. A., & K. D. Putirka (2017), A new clinopyroxene-liquid barometer, and implications for magma storage pressures under Icelandic rift zones, *American Mineralogist*, 102, 777–794, doi:10.2138/am-2017-5968.

Neave, D. A., E. Passmore, J. Maclennan, J. G. Fitton, & T. Thordarson (2013), Crystal-melt relationships and the record of deep mixing and crystallization in the AD 1783

Laki eruption, Iceland, *Journal of Petrology*, 54(8), 1661–1690, doi:10.1093/petrology/egt027.

Neave, D. A., J. Maclennan, M. Edmonds, & T. Thordarson (2014), Melt mixing causes negative correlation of trace element enrichment and CO$_{2}$ content prior to an Icelandic eruption, *Earth and Planetary Science Letters*, 400, 272–283, doi:10.1016/j.epsl.2014.05.050.

Neave, D. A., E. Bali, G. H. Guðfinnsson, S. A. Halldórsson, M. Kahl, A.-S. Schmidt, & F. Holtz (2019a), Clinopyroxene–liquid equilibria and geothermobarometry in natural and experimental tholeiites: the 2014–2015 Holuhraun eruption, Iceland, *Journal of Petrology*, 60, 1653–1680, doi:10.1093/petrology/egz042.

Neave, D. A., O. Namur, O. Shorttle, & F. Holtz (2019b), Magmatic evolution biases basaltic records of mantle chemistry towards melts from recycled sources, *Earth and Planetary Science Letters*, 520, 199–211, doi:10.1016/j.epsl.2019.06.003.

Neave, D. A., A. G. Stewart, M. E. Hartley, & C. McCammon (2024a), Re-evaluating stoichiometric estimates of iron valence in magmatic clinopyroxene crystals, *Contributions to Mineralogy and Petrology*, 179(5), 17, doi:10.1007/s00410-023-02080-2.

Neave, D. A., A. G. Stewart, M. E. Hartley, & O. Namur (2024b), Iron valence systematics in clinopyroxene crystals from ocean island basalts, *Contributions to Mineralogy and Petrology*, 179(6), 67, doi:10.1007/s00410-024-02144-x.

Nicklas, R., R. Hahn, & J. Day (2022a), Oxidation of La Réunion lavas with MORB-like fO2 by assimilation, *Geochemical Perspectives Letters*, 20, 32–36, doi:10.7185/geochemlet.2205.

Nicklas, R. W., R. K. Hahn, L. N. Willhite, M. G. Jackson, V. Zanon, R. Arevalo, & J. M. Day (2022b), Oxidized mantle sources of HIMU- and EM-type Ocean Island Basalts, *Chemical Geology*, 602, 120,901, doi:10.1016/j.chemgeo.2022.120901.

Novella, D., J. Maclennan, O. Shorttle, J. Prytulak, & B. J. Murton (2020), A multi-proxy investigation of mantle oxygen fugacity along the Reykjanes Ridge, *Earth and Planetary Science Letters*, 531, 115,973, doi:10.1016/j.epsl.2019.115973.

Palin, R. M., O. M. Weller, D. J. Waters, & B. Dyck (2016), Quantifying geological uncertainty in metamorphic phase equilibria modelling; a Monte Carlo assessment and implications for tectonic interpretations, *Geoscience Frontiers*, 7(4), 591–607, doi:10.1016/j.gsf.2015.08.005.

Passmore, E., J. Maclennan, J. G. Fitton, & T. Thordarson (2012), Mush disaggregation in basaltic magma chambers: Evidence from the AD 1783 Laki eruption, *Journal of Petrology*, 53(12), 2593–2623, doi:10.1093/petrology/egs061.

Pilet, S., P. Ulmer, & S. Villiger (2010), Liquid line of descent of a basanitic liquid at 1.5 GPa: constraints on the formation of metasomatic veins, *Contributions to Mineralogy and Petrology*, 159(5), 621–643, doi:10.1007/s00410-009-0445-y.

Powell, R., & T. J. B. Holland (2008), On thermobarometry, *Journal of Metamorphic Geology*, 26(2), 155–179, doi:10.1111/j.1525-1314.2007.00756.x.

Powell, R., T. J. B. Holland, & N. Worley (1998), Calculating phase diagrams involving solid solutions via non-linear equations, with examples using THERMOCALC, *Journal of Metamorphic Geology*, 16, 577–588, doi:10.1111/j.1525-1314.1998.00157.x.

Putirka, K. D. (2008), Thermometers and Barometers for Volcanic Systems, *Reviews in Mineralogy and Geochemistry*, 69(1), 61–120, doi:10.2138/rmg.2008.69.3.

Riel, N., B. J. P. Kaus, E. C. R. Green, & N. Berlie (2022), MAGEMin, an Efficient Gibbs Energy Minimizer: Application to Igneous Systems, *Geochemistry, Geophysics, Geosystems*, 23(7), 1–27, doi:10.1029/2022GC010427.

Salazar-Naranjo, A. F., & S. R. F. Vlach (2023), New experimental constraints for the evolution and thermobarometry of alkali ultrabasic to intermediate igneous rocks, *Journal of Petrology*, p. egad078, doi:10.1093/petrology/egad078.

Saper, L. M., M. B. Stolper, & E. M. Baker (2022), Fe^{2+}–Mg partitioning between olivine and liquid at low oxygen fugacity: an experimental and thermodynamic framework, *Contributions to Mineralogy and Petrology*, 177, 94, doi:10.1007/s00410-022-01955-0.

Shepherd, K., O. Namur, M. J. Toplis, J.-L. Devidak, & B. Charlier (2022), Trace element partitioning between clinopyroxene, magnetite, ilmenite and ferrobasaltic to dacitic magmas: an experimental study on the role of oxygen fugacity and melt composition, *Contributions to Mineralogy and Petrology*, 177, 90, doi:10.1007/s00410-022-01957-y.

Shorttle, O. (2015), Geochemical variability in MORB controlled by concurrent mixing and crystallisation, *Earth and Planetary Science Letters*, 424, 1–14, doi:10.1016/j.epsl.2015.04.035.

Sisson, T. W., & T. L. Grove (1993), Experimental investigations of the role of H_2O in calc-alkaline differentiation and subduction zone magmatism, *Contributions to Mineralogy and Petrology*, 113(2), 143–166, doi:10.1007/BF00283225.

Sobolev, V. N., C. A. Mccammon, L. A. Taylor, G. A. Snyder, & N. V. Sobolev (1999), Precise Mössbauer milliprobe determination of ferric iron in rock-forming minerals and limitations of electron microprobe analysis, *American Mineralogist*, 84, 78–85.

Taracsák, Z., M.-A. Longpré, R. TartÃÍse, R. Burgess, M. Edmonds, & M. E. Hartley (2022), Highly oxidising conditions in volatile-rich El Hierro magmas: implications for ocean island magmatism, *Journal of Petrology*, 63, 1–21, doi:10.1093/petrology/egac011.

Tomlinson, E. L., & T. J. B. Holland (2021), A Thermodynamic Model for the Subsolidus Evolution and Melting of Peridotite, *Journal of Petrology*, 62(1), egab012, doi:10.1093/petrology/egab012.

Toplis, M. J. (2005), The thermodynamics of iron and magnesium partitioning between olivine and liquid: Criteria for assessing and predicting equilibrium in natural and experimental systems, *Contributions to Mineralogy and Petrology*, 149(1), 22–39, doi:10.1007/s00410-004-0629-4.

Toplis, M. J., & M. R. Carroll (1995), An Experimental Study of the Influence of Oxygen Fugacity on Fe-Ti Oxide Stability, Phase Relations, and Mineral-Melt Equilibria in Ferro-Basaltic Systems, *Journal of Petrology*, 36(5), 1137–1170.

Ubide, T., C. Galé, P. Larrea, E. Arranz, & M. Lago (2014), Antecrysts and their effect on rock compositions: The Cretaceous lamprophyre suite in the Catalonian Coastal Ranges (NE Spain), *Lithos*, 206-207, 214–233, doi:10.1016/j.lithos.2014.07.029.

Ubide, T., S. Mollo, J.-X. Zhao, M. Nazzari, & P. Scarlato (2019), Sector-zoned clinopyroxene as a recorder of magma history, eruption triggers, and ascent rates, *Geochimica et Cosmochimica Acta*, 251, 265–283, doi:10.1016/j.gca.2019.02.021.

Ubide, T., P. Larrea, L. Becerril, & C. Galé (2022), Volcanic plumbing filters on ocean-island basalt geochemistry, *Geology*, 50, 26–31, doi:10.1130/G49224.1.

van Gerve, T. D., D. A. Neave, P. Wieser, H. Lamadrid, N. Hulsbosch, & O. Namur (2024), The origin and differentiation of CO_2-rich primary melts in Ocean Island volcanoes: Integrating 3D X-ray tomography with chemical microanalysis of olivine-hosted melt inclusions from Pico (Azores), *Journal of Petrology*, 65, 1–24, doi:10.1093/petrology/egae006.

Watson, E. B. (1979), Apatite saturation in basic to intermediate magmas, *Geophysical Research Letters*, 6(12), 937–940, doi:10.1029/GL006i012p00937.

Weller, O. M., M. R. St-Onge, D. J. Waters, N. Rayner, M. P. Searle, S. L. Chung,

R. M. Palin, Y. H. Lee, & X. Xu (2013), Quantifying Barrovian metamorphism in the Danba Structural Culmination of eastern tibet, *Journal of Metamorphic Geology*, 31(9), 909–935, doi:10.1111/jmg.12050.

Weller, O. M., T. J. B. Holland, C. R. Soderman, E. C. R. Green, R. Powell, C. D. Beard, & N. Riel (2024), New thermodynamic models for anhydrous alkaline-silicate magmatic systems, *Journal of Petrology*, p. egae098, doi:10.1093/petrology/egae098.

Wieser, P. E., A. J. R. Kent, & C. B. Till (2023), Barometers Behaving Badly II: a Critical Evaluation of Cpx-Only and Cpx-Liq Thermobarometry in Variably-Hydrous Arc Magmas, *Journal of Petrology*, 64(8), egad050, doi:10.1093/petrology/egad050.

Wood, B. J., & J. D. Blundy (1997), A predictive model for rare earth element partitioning between clinopyroxene and anhydrous silicate melt, *Contributions to Mineralogy and Petrology*, 129(2-3), 166–181, doi:10.1007/s004100050330.

Wood, B. J., L. T. Bryndzia, & K. E. Johnson (1990), Mantle oxidation state and its relationship to tectonic environment and fluid speciation, *Science*, 248(4953), 337.

Table 1: Whole-rock data (wt.%) from our target systems. Data sources: Holuhraun—mean whole-rock composition from Halldórsson *et al.* (2018); Laki—mean whole-rock composition from Passmore *et al.* (2012); PI-011 and PI-041—Pico whole-rock compositions from van Gerve *et al.* (2024).

	Holuhraun	Laki	Pico - PI-011	Pico - PI-041
SiO_2	50.00	50.28	48.86	46.29
TiO_2	1.88	2.75	2.35	3.55
Al_2O_3	13.79	13.74	13.81	17.19
FeO^T	12.35	13.42	9.83	10.99
MnO	0.21	0.22	0.17	0.17
MgO	6.82	5.78	10.24	6.22
CaO	12.01	10.41	10.45	9.44
Na_2O	2.44	2.69	2.87	2.70
K_2O	0.20	0.42	1.22	1.08
P_2O_5	0.17	0.29	0.47	0.61

Table 2: THERMOCALC inputs (expressed on a molar basis). FeO^T = total FeO. THERMOCALC treats Fe_2O_3 as 2FeO + O. Therefore, $X_{Fe^{3+}} = 2O/FeO^T$ and Mg# = MgO/(MgO + FeO^T - 2O). PI = peralkaline index = $(Na_2O + K_2O)/Al_2O_3$.

Sample	SiO_2	TiO_2	Al_2O_3	CaO	MgO	FeO^T	K_2O	Na_2O	O	$X_{Fe^{3+}}$	Mg#	PI
Holuhraun	52.41	1.48	8.52	13.49	10.66	10.83	0.13	2.48	0.00	0.00	0.50	0.31
Holuhraun	52.41	1.48	8.52	13.49	10.66	10.83	0.13	2.48	2.71	0.50	0.66	0.31
Laki	53.31	2.19	8.58	11.83	9.14	11.9	0.28	2.76	0.00	0.00	0.43	0.35
Laki	53.31	2.19	8.58	11.83	9.14	11.9	0.28	2.76	2.98	0.50	0.61	0.35
Pico - PI-011	50.37	1.82	8.39	11.54	15.74	8.47	0.80	2.87	0.00	0.00	0.65	0.44
Pico - PI-011	50.37	1.82	8.39	11.54	15.74	8.47	0.80	2.87	2.12	0.50	0.79	0.44
Pico - PI-041	50.88	2.94	11.13	11.12	10.19	10.1	0.76	2.88	0.00	0.00	0.50	0.33
Pico - PI-041	50.88	2.94	11.13	11.12	10.19	10.1	0.76	2.88	2.53	0.50	0.67	0.33

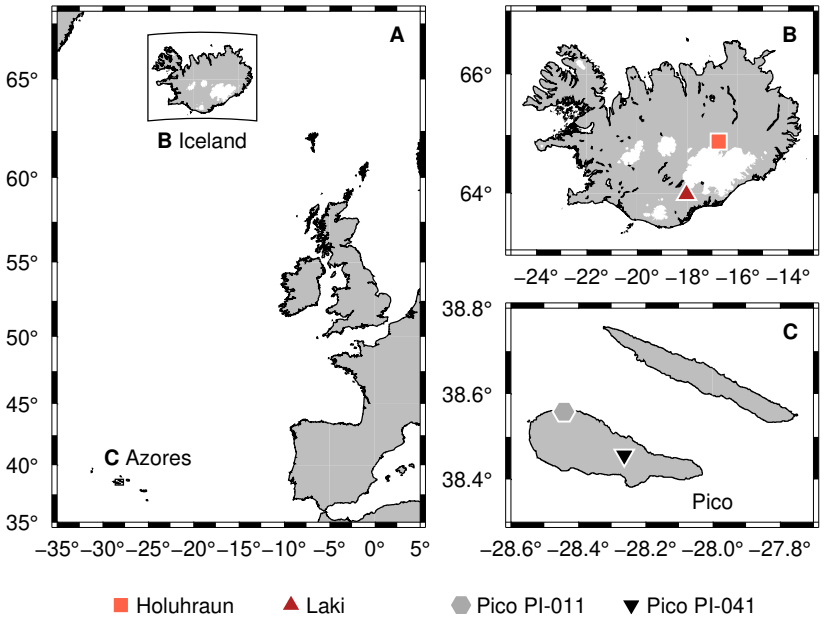

Figure 1: (A) Map of the North Atlantic region encompassing sample locations in Iceland and the Azores. (B) Map of Iceland showing sample locations. Laki is represented by basalt lava sample LAK-04 described by Passmore *et al.* (2012) and Neave *et al.* (2013). Holuhraun is represented by a tephra sample equivalent to sample H14 described by Halldórsson *et al.* (2018) and literature data from across lava flow reported by Halldórsson *et al.* (2018). (C) Map of part of the Azores archipelago showing sample locations on Pico Island (van Gerve *et al.*, 2024). PI-011 is a lava sample and PI-041 is a tephra sample.

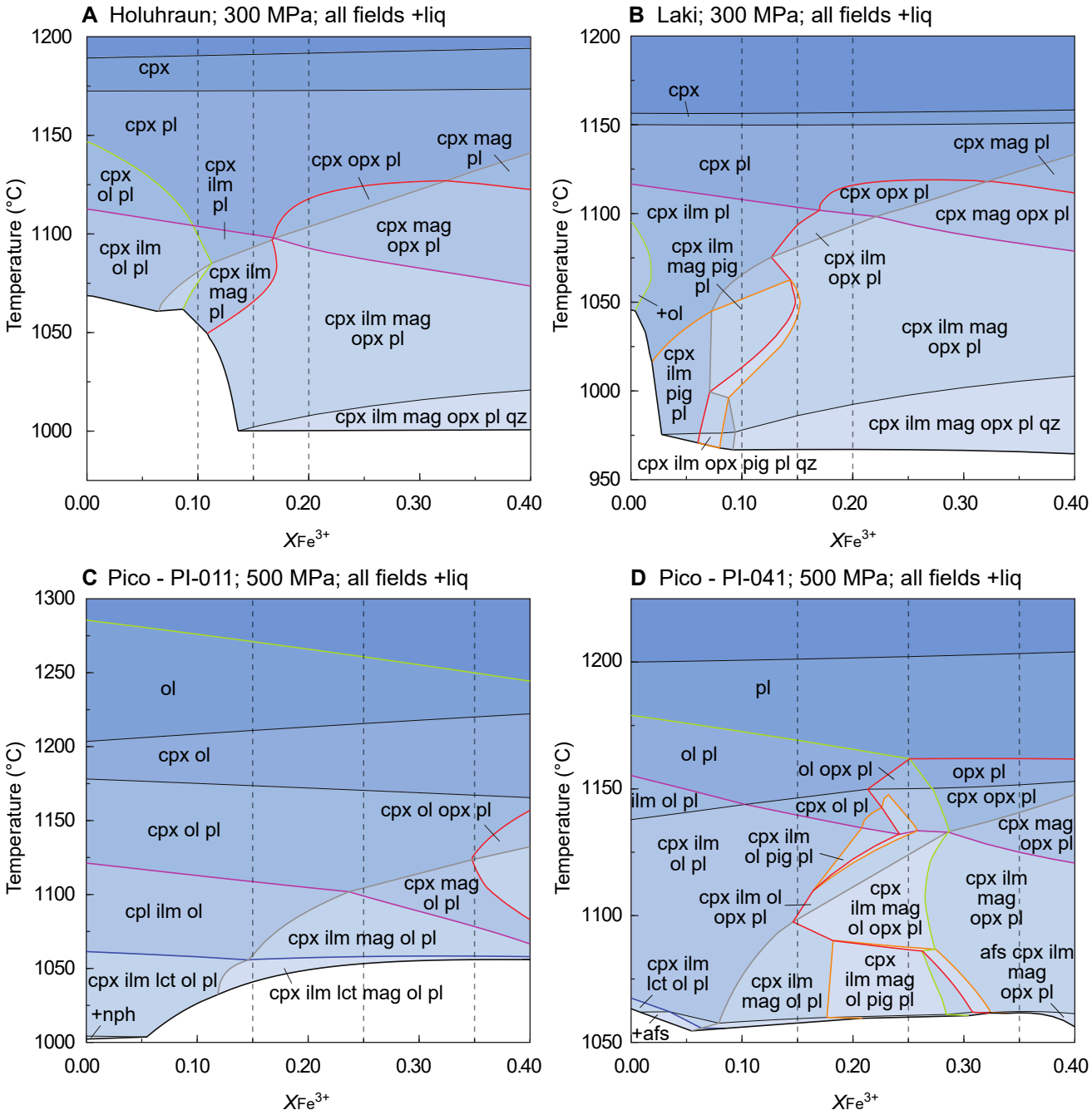

Figure 2: Pseudosections calculated from whole-rock compositions documented in Table 1. Pseudosections were calculated at fixed pressures, superliquidus to solidus temperatures and $X_{Fe^{3+}}$ values (i.e., bulk $Fe^{3+}/\Sigma Fe$ contents) varying between 0 and 0.4. Vertical dashed lines show the $X_{Fe^{3+}}$ values for which further parameters are plotted in Figs. 4–7. (A) Pseudosection calculated at 300 MPa for the mean Holuhraun whole-rock composition reported by Halldórsson *et al.* (2018). (B) Pseudosection calculated at 300 MPa for the mean Laki whole-rock composition reported by Passmore *et al.* (2012). (C) and (D) Pseudosection calculated at 500 MPa for the whole-rock compositions of samples PI-011 and PI-041 from Pico island in the Azores reported by van Gerve *et al.* (2024).

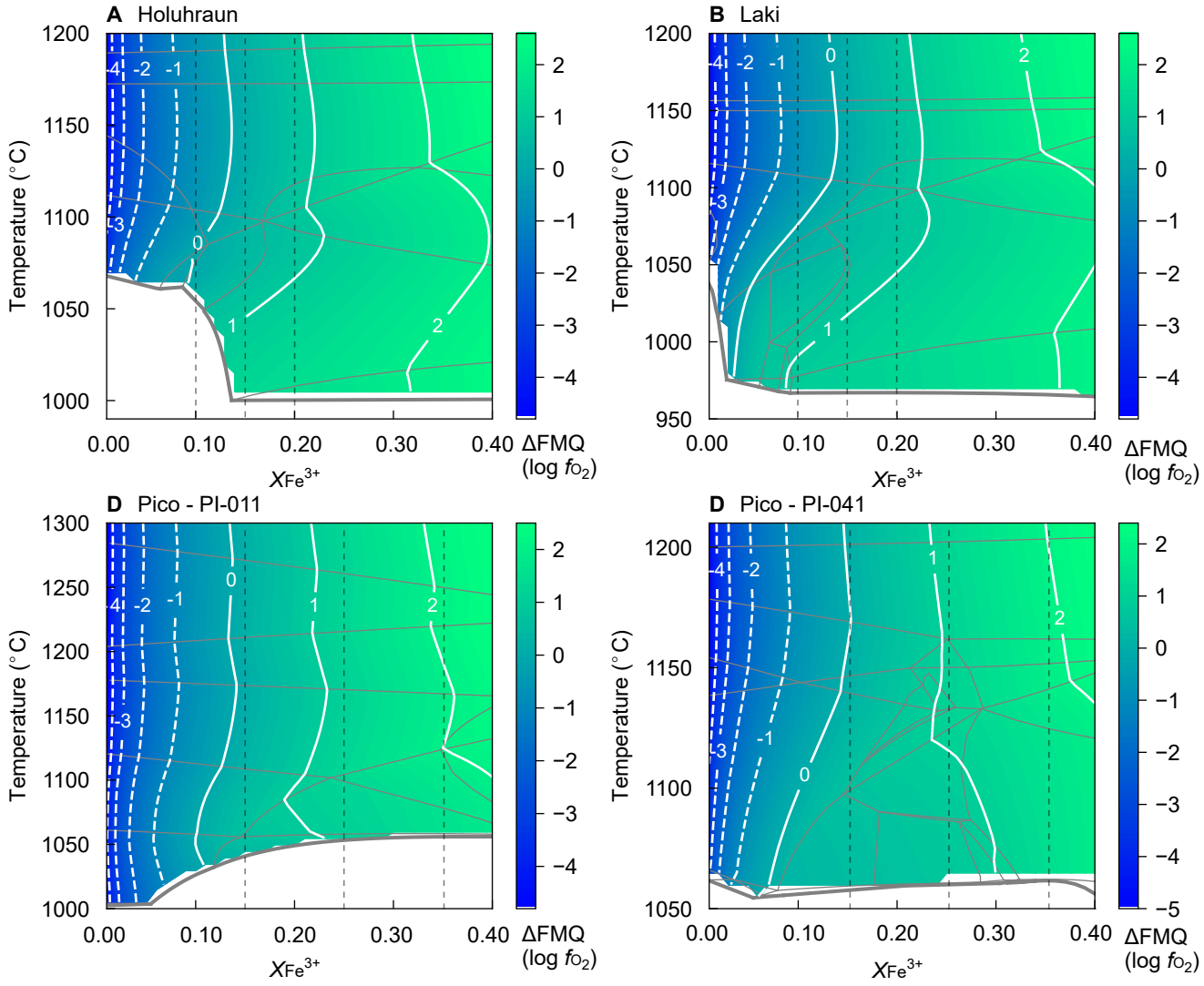

Figure 3: Pseudosections presented in Fig. 2 contoured for oxygen fugacity (f_{O_2}) reported as log unit deviations from fayalite-magnetite-quartz equilibrium (ΔFMQ). Vertical dashed lines show the $X_{Fe^{3+}}$ values for which further parameters are plotted in Figs. 4–7.

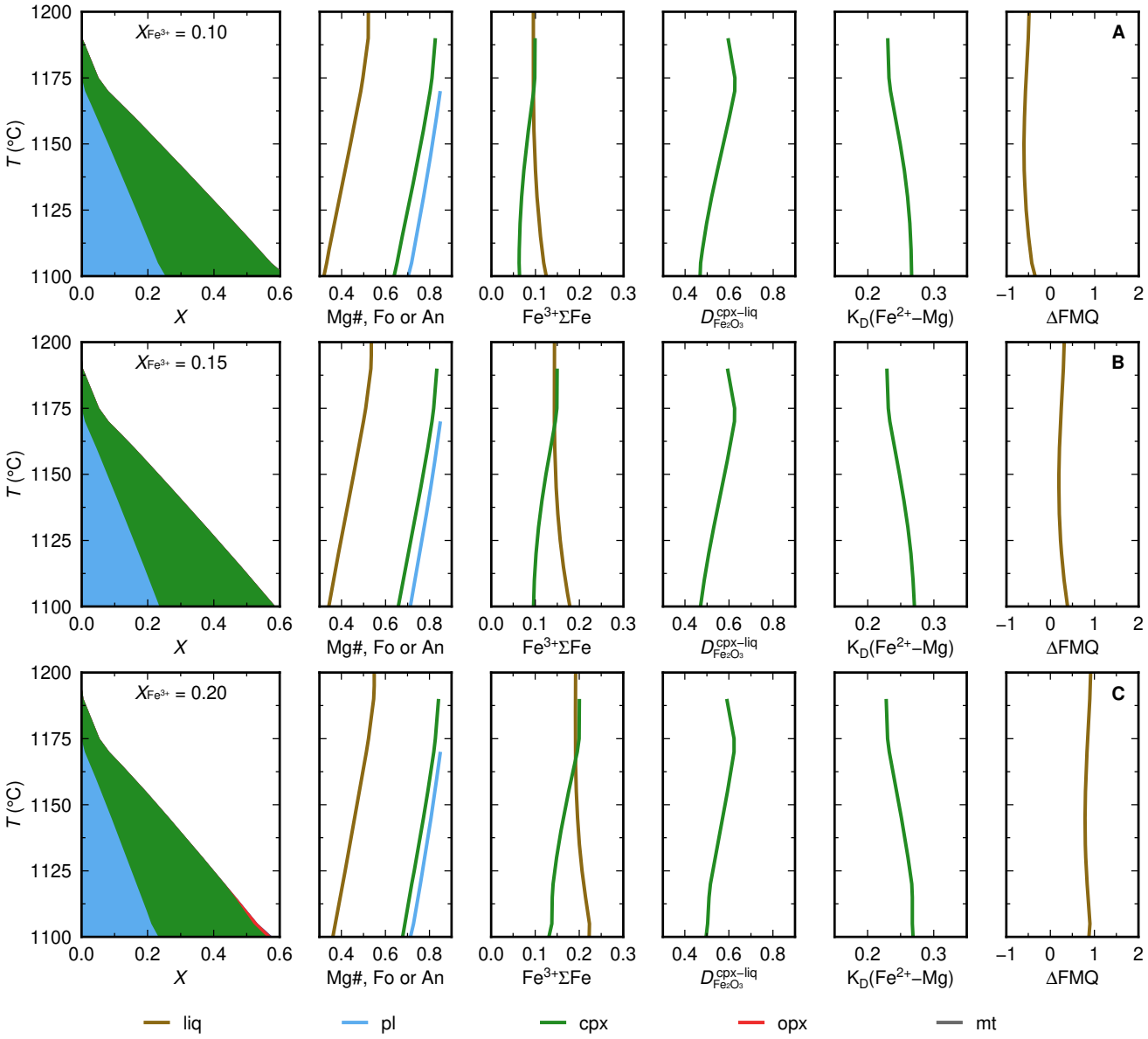

Figure 4: Plots summarising phase proportions, phase compositions, Fe(-Mg) partitioning and oxygen fugacity (f_{O_2}) systematics calculated for our Holuhraun composition at a range of $X_{Fe^{3+}}$ values. Results from slices at $X_{Fe^{3+}}$ values of 0.1, 0.15 and 0.2 are shown in (A), (B) and (C) respectively.

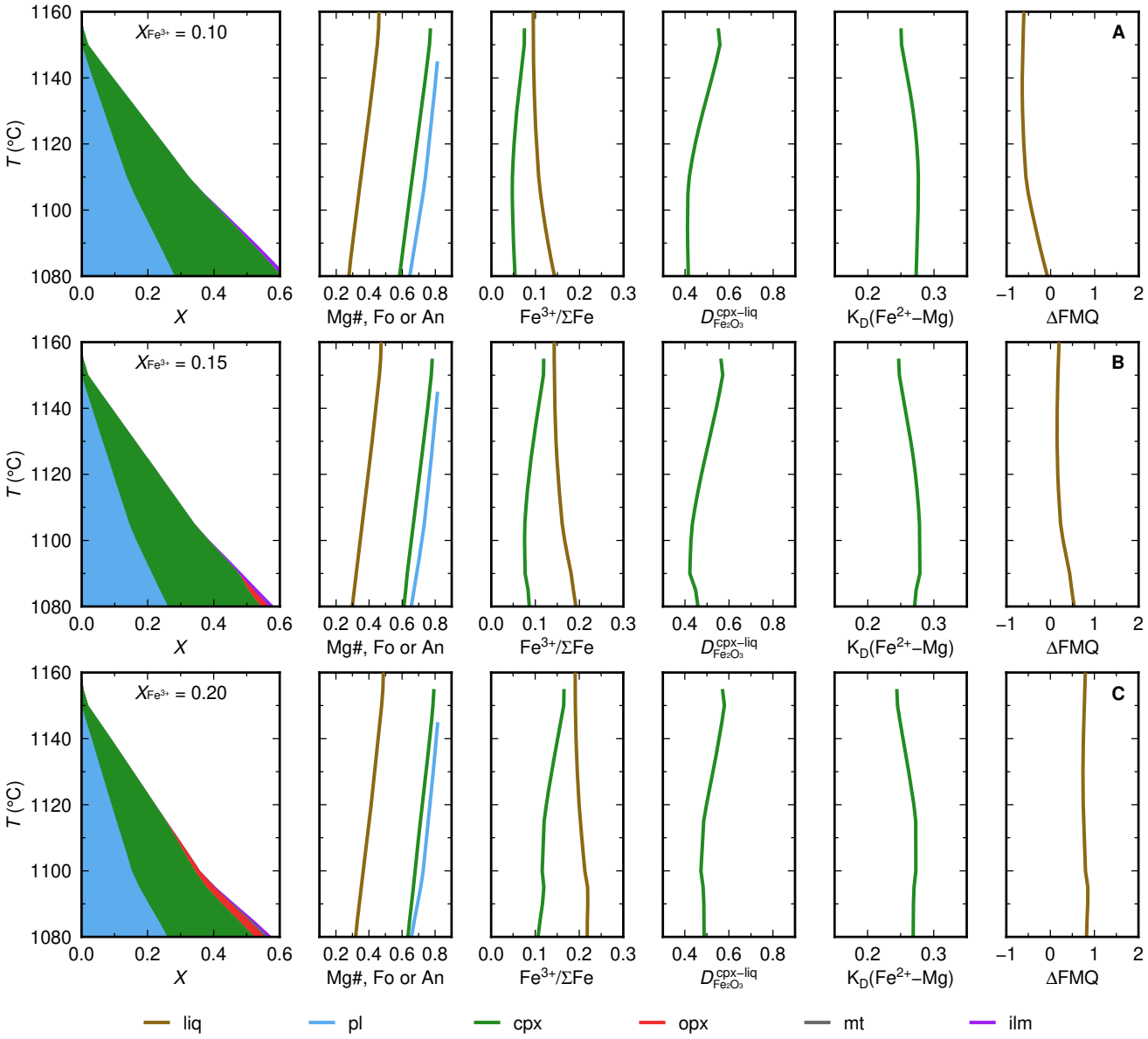

Figure 5: Plots summarising phase proportions, phase compositions, Fe(-Mg) partitioning and oxygen fugacity (f_{O_2}) systematics calculated for our Laki composition at a range of $X_{Fe^{3+}}$ values. Results from slices at $X_{Fe^{3+}}$ values of 0.1, 0.15 and 0.2 are shown in (A), (B) and (C) respectively.

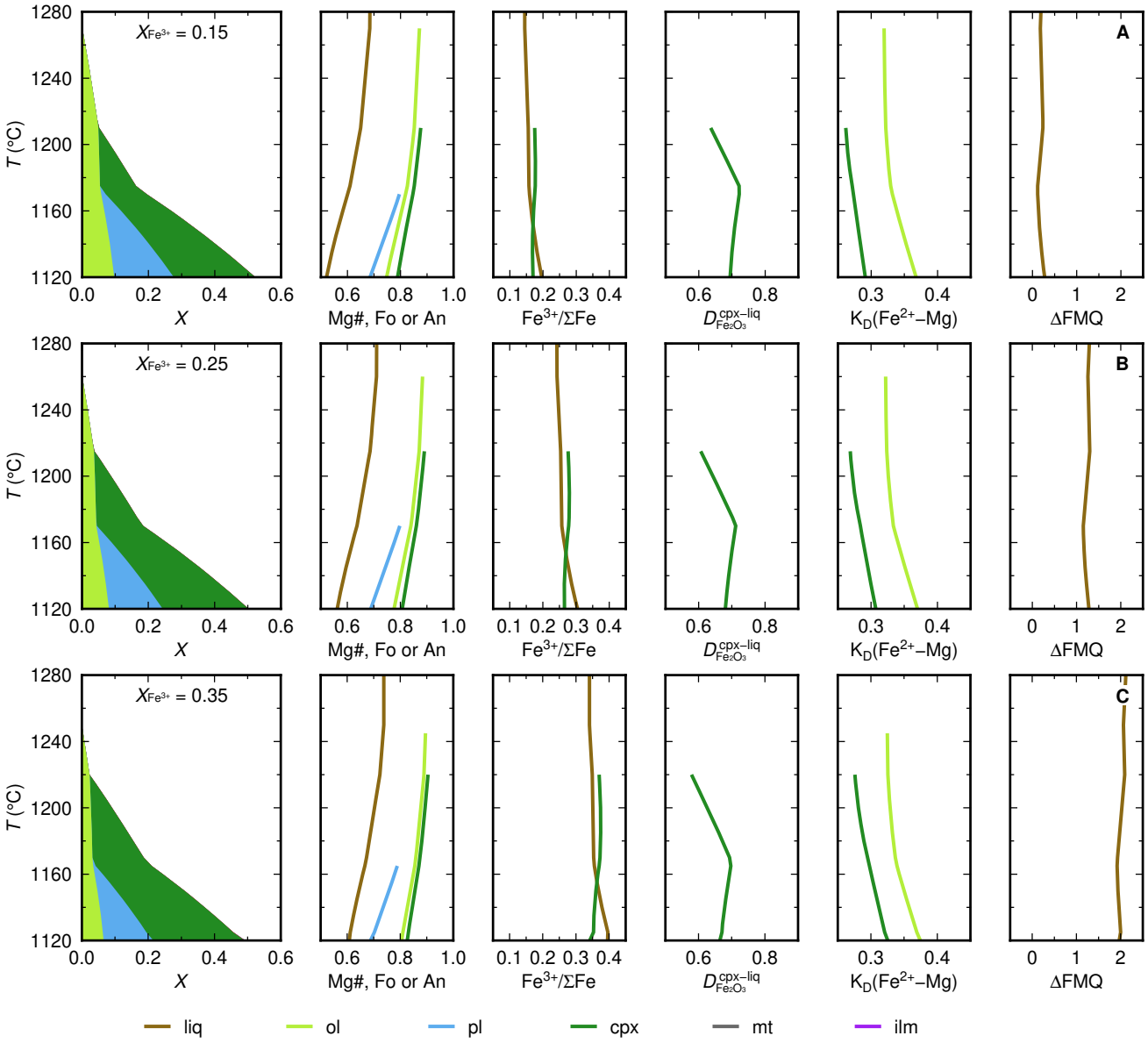

Figure 6: Plots summarising phase proportions, phase compositions, Fe(-Mg) partitioning and oxygen fugacity (f_{O_2}) systematics calculated for composition PI-011 from Pico at a range of values contents. Results from slices at $X_{Fe^{3+}}$ values of 0.15, 0.25 and 0.35 are shown in (A), (B) and (C) respectively.

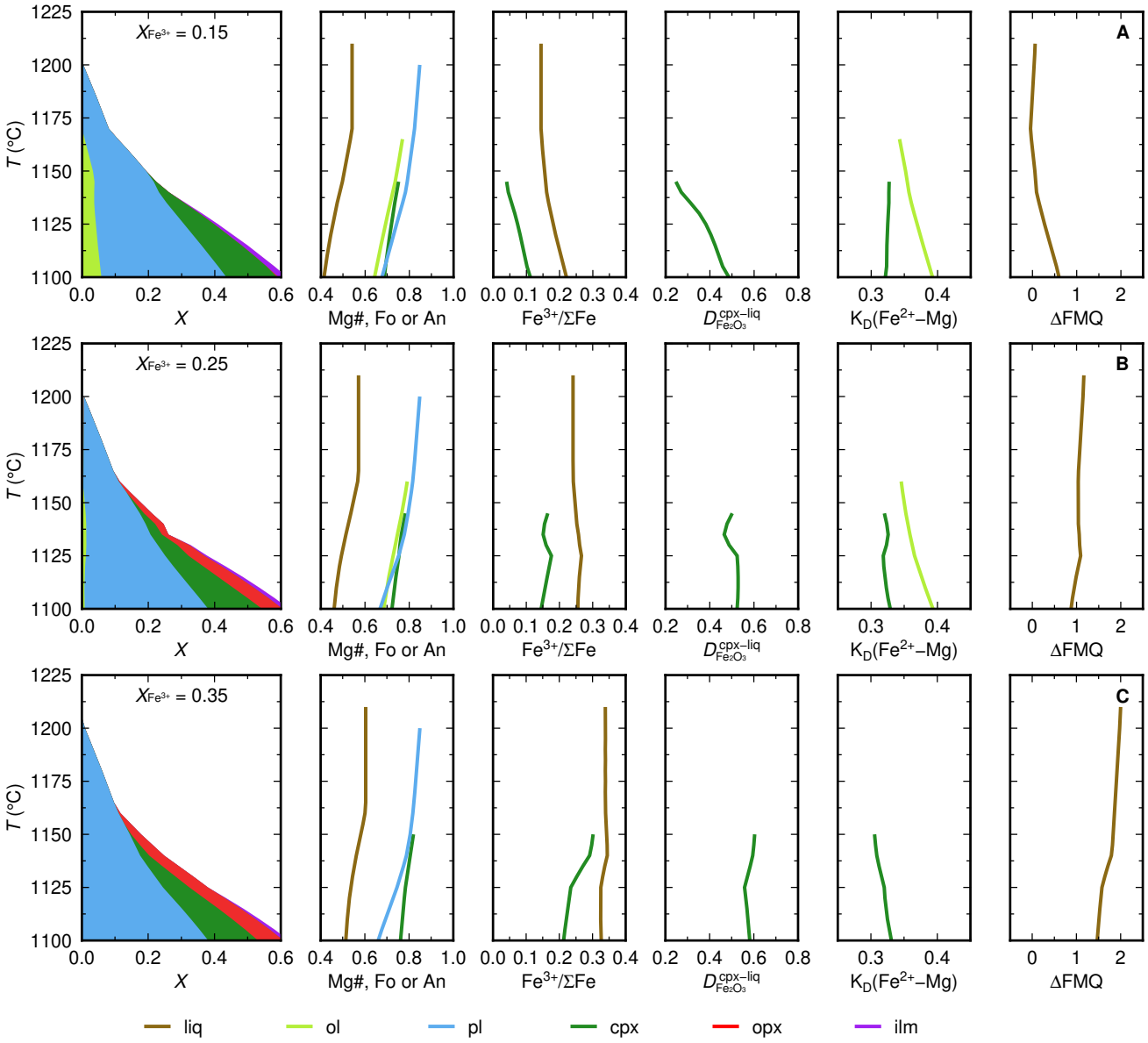

Figure 7: Plots summarising phase proportions, phase compositions, Fe(-Mg) partitioning and oxygen fugacity (f_{O_2}) systematics calculated for composition PI-041 from Pico at a range of $X_{Fe^{3+}}$ values. Results from slices at $X_{Fe^{3+}}$ values of 0.15, 0.25 and 0.35 are shown in (A), (B) and (C) respectively.

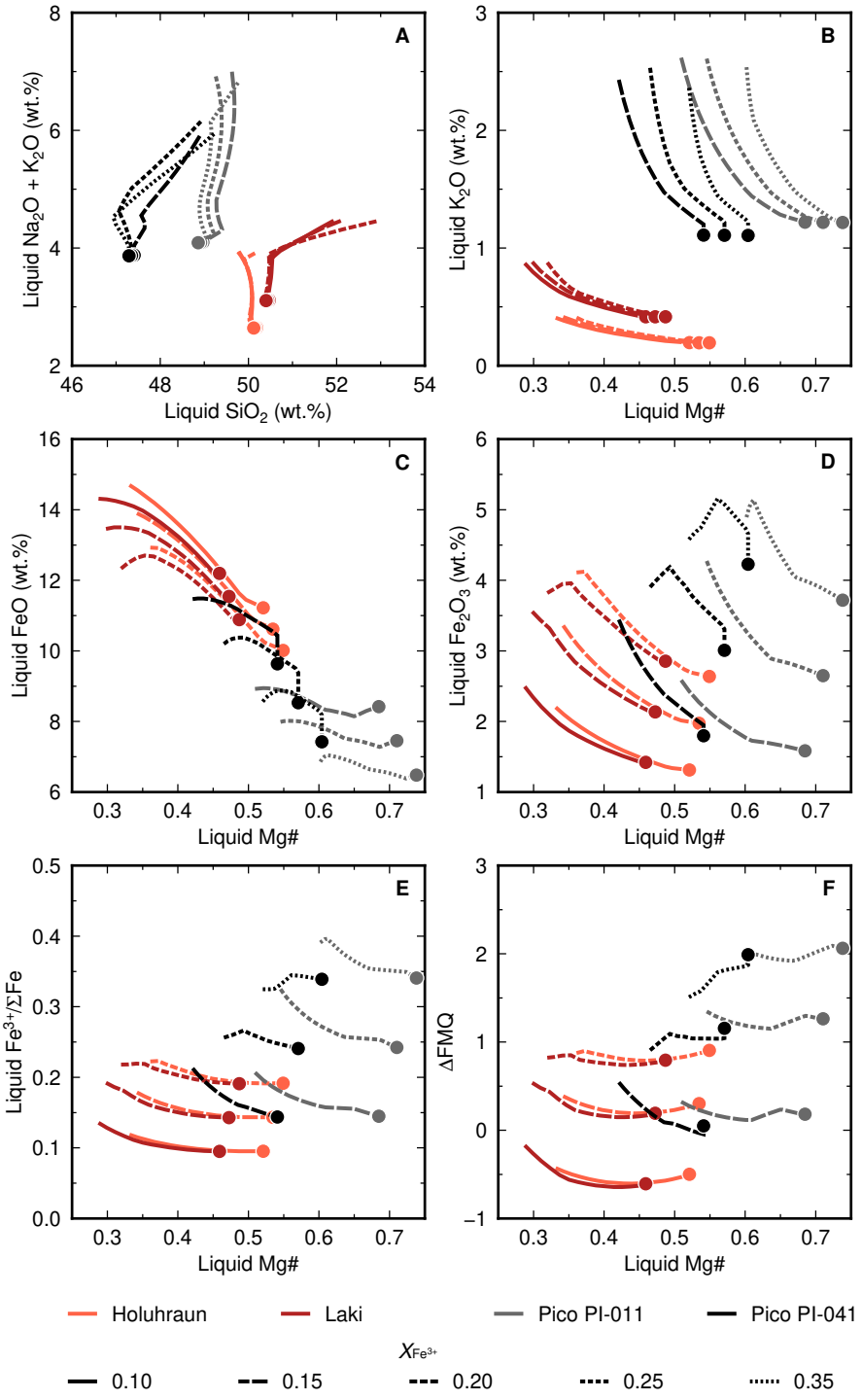

Figure 8: Plots summarising evolution trajectories of modelled liquid compositions (i.e., liquid lines of descent) from superliquidus conditions to a liquid modal proportion of ∼0.4 at a range of $X_{Fe^{3+}}$ values. Circles show bulk compositions (i.e., superliquidus compositions). Panels show liquid Mg# (Mg/(Mg+Fe^{2+}) on a molar basis) versus (A) liquid total alkalis (Na_2O + K_2O), (B) liquid K_2O, (C) liquid FeO, (D) liquid Fe_2O_3, (E) liquid $Fe^{3+}/\Sigma Fe$ and (F) oxygen fugacity (f_{O_2}) expressed as log unit deviations from fayalite-magnetite-quartz equilibrium (ΔFMQ).

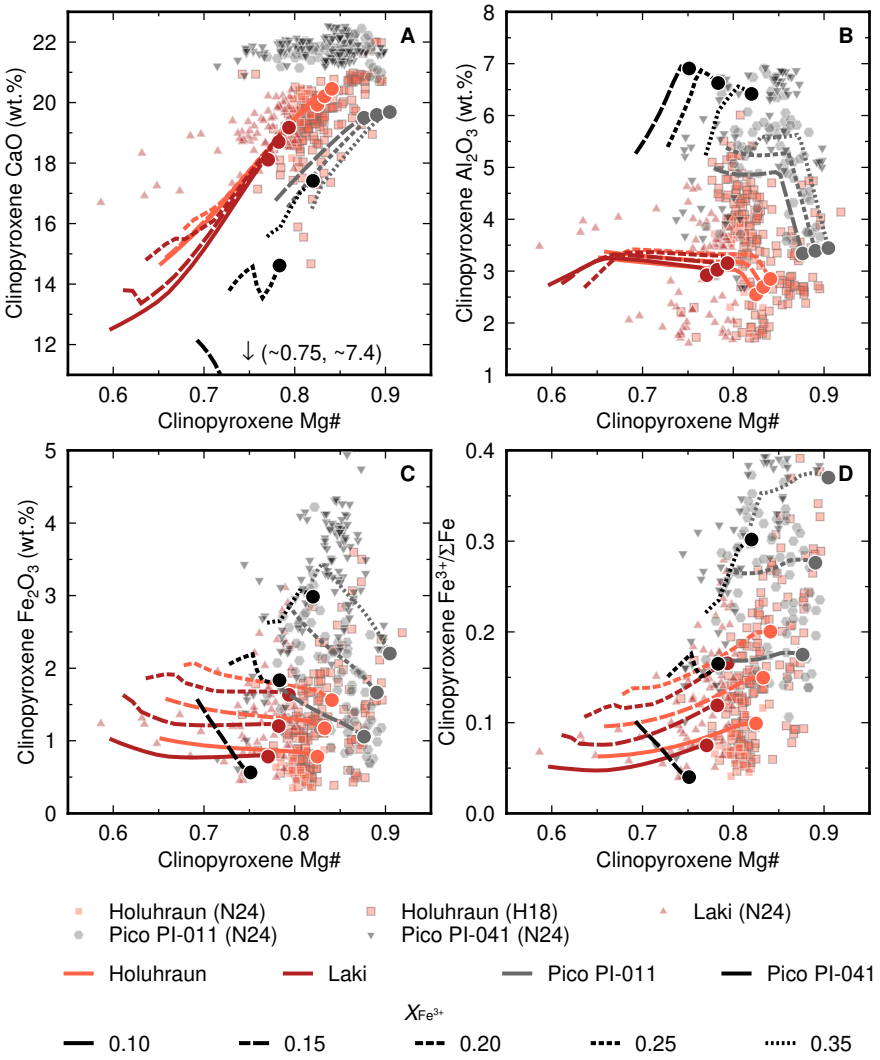

Figure 9: Plots summarising evolution trajectories of modelled clinopyroxene compositions (i.e., crystal lines of descent) from the clinopyroxene liquidus to a liquid modal proportion of ∼0.4 at a range of $X_{Fe^{3+}}$ values. Circles show liquidus clinopyroxene compositions. Natural compositions from Halldórsson *et al.* (2018) and Neave *et al.* (2024b) are shown. Data from Halldórsson *et al.* (2018)—H18—are less precise than those from Neave *et al.* (2024b) but cover a much greater diversity of eruption products and are generally from larger clinopyroxene crystals. Panels show clinopyroxene Mg# ($Mg/(Mg+Fe^{2+})$ on a molar basis) versus (A) clinopyroxene CaO, (B) clinopyroxene Al_2O_3, (C) clinopyroxene Fe_2O_3 and (D) clinopyroxene $Fe^{3+}/\Sigma Fe$.

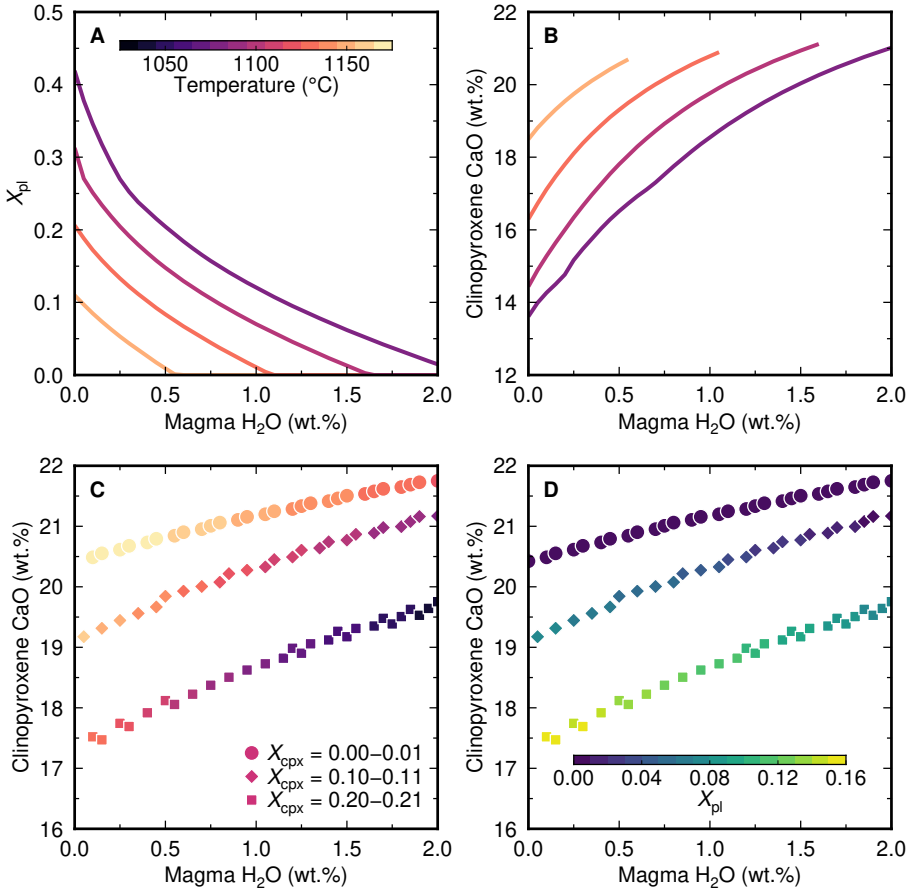

Figure 10: Plots showing the effect of magmatic H_2O on plagioclase and clinopyroxene equilibria calculated for our Holuhraun composition at a fixed $X_{Fe^{3+}}$ of 0.15 and magma H_2O contents of 0 to 2 wt.%. (A) Plagioclase modal proportion as a function of temperature and magma H_2O content; as the magma H_2O content increases at any given temperature, the stability of plagioclase decreases. (B) Clinopyroxene CaO contents as a function of temperature and magma H_2O content; at any given temperature, the CaO content of clinopyroxene increases with increasing magma H_2O content. (C and D) Clinopyroxene CaO contents as a function of clinopyroxene modal proportion, magma H_2O content and (C) temperature and (D) plagioclase modal proportion (D); at any given modal proportion of clinopyroxene, the CaO content of clinopyroxene increases and the equilibrium model proportion of plagioclase decreases as magma H_2O content increases.

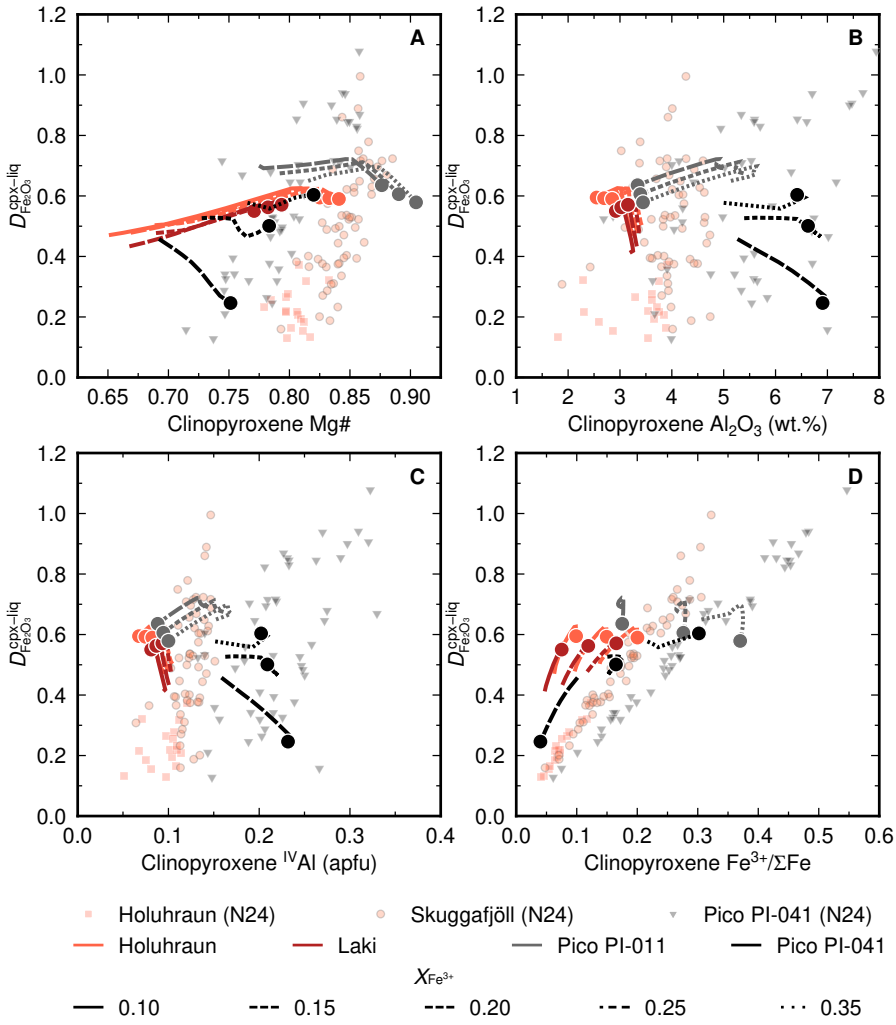

Figure 11: Plots summarising $D^{\mathrm{cpx-liq}}_{\mathrm{Fe_2O_3}}$ values calculated from thermodynamic models (from the clinopyroxene liquidus to a liquid modal proportion of ∼0.4) and natural observations as functions of clinopyroxene compositions. Circles show values at the clinopyroxene liquidus. Panels show $D^{\mathrm{cpx-liq}}_{\mathrm{Fe_2O_3}}$ values as functions of (A) clinopyroxene Mg# (Mg/(Mg+Fe^{2+}) on a molar basis), (B) clinopyroxene Al_2O_3, (C) clinopyroxene $^{\mathrm{IV}}$Al and (D) clinopyroxene $Fe^{3+}/\Sigma Fe$.

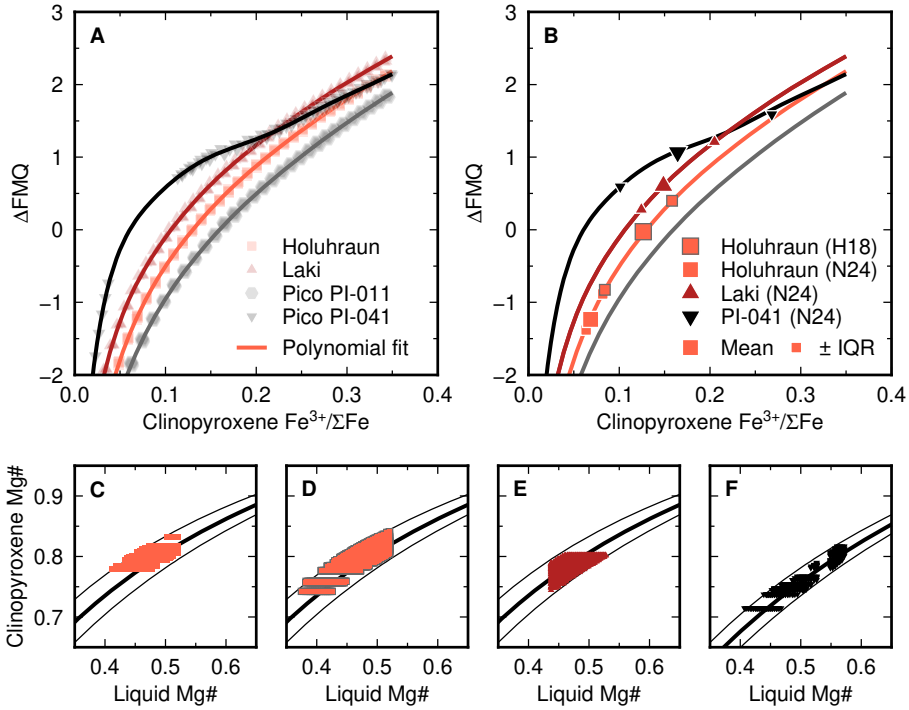

Figure 12: Plots summarising magmatic oxygen fugacity (f_{O_2}) conditions estimated from natural clinopyroxene $Fe^{3+}/\Sigma Fe$ contents using relationships between clinopyroxene $Fe^{3+}/\Sigma Fe$ and f_{O_2} parameterised from calculated near-liquidus clinopyroxene compositions; clinopyroxene is considered to be near-liquidus when it makes up $\leq$5 modal % of the system). Oxygen fugacity conditions are expressed as log-unit deviations from the fayalite-magnetite-quartz equilibrium (ΔFMQ). Natural clinopyroxene compositions from Halldórsson *et al.* (2018) and Neave *et al.* (2024b) were filtered to return $K_{D,Fe^{2+}-Mg}^{cpx-liq}$ values within 0.03 of values calculated using the bulk as the liquid composition (typically 0.24 for tholeiitic compositions from Holuhraun and Laki and 0.30 for alkali compositions from Pico). No fits were found for clinopyroxene crystals in sample PI-011 from Pico, likely because the bulk composition has accumulated olivine; the other modelled compositions were matrix glasses. Clinopyroxene crystals from the Holuhraun and Laki lava return median f_{O_2} conditions of ΔFMQ to ΔFMQ+0.7 that are within half a log unit of published values for these eruptions (Bali *et al.*, 2018; Hartley *et al.*, 2017); small clinopyroxene crystals from a tephra sample return more reducing conditions of ΔFMQ-1 potentially indicative of crystallisation after appreciable reductive SO_2 degassing. Clinopyroxene crystals in sample PI-041 from Pico return median f_{O_2} conditions of ΔFMQ+1.1, lower than values for similar compositions erupted at other ocean islands (Moussallam *et al.*, 2019) and estimated from olivine-liquid equilibrium (Neave *et al.*, 2024b), and thus feasibly compromised by reductive SO_2 degassing.